Czech Technical University in Prague
Faculty of Nuclear Sciences and Physical Engineering

Doctoral Thesis

Investigation of Functional Thin Films Prepared by Ionized Jet Deposition Method

Prague 2023

Jakub Skočdopole

This thesis is submitted to the Faculty of Nuclear Sciences and Physical Engineering, Czech Technical University in Prague, in partial fulfilment of the requirements for the degree of Doctor of Philosophy (Ph.D.) in Physical Engineering.

Copyright © 2023 Jakub Skočdopole. All Rights Reserved.

Bibliografický záznam

Autor	Ing. Jakub Skočdopole, České vysoké učení technické v Praze, Fakulta jaderná a fyzikálně inženýrská, Katedra inženýrství pevných látek
Název práce	Výzkum tenkých funkčních vrstev připravených metodou ionizační tryskové depozice
Studijní program	Aplikace přírodních věd
Studijní obor	Fyzikální inženýrství
Školitel	doc. Ing. Ladislav Kalvoda, CSc. České vysoké učení technické v Praze, Fakulta jaderná a fyzikálně inženýrská, Katedra inženýrství pevných látek
Akademický rok	2023
Počet stran	103
Klíčová slova	příprava tenkých vrstev, charakterizace tenkých vrstev, metoda Ionized Jet Deposition, vysokoteplotní supravodiče, skenovací elektronová mikroskopie, rentgenová difrakce

Bibliographic Entry

Author	Ing. Jakub Skočdopole, Czech Technical University in Prague, Faculty of Nuclear Sciences and Physical Engineering, Department of Solid State Engineering
Title of dissertation	Investigation of Functional Thin Films Prepared by Ionized Jet Deposition Method
Degree programme	Application of Natural Sciences
Field of study	Physical Engineering
Supervisor	doc. Ing. Ladislav Kalvoda, CSc. Czech Technical University in Prague, Faculty of Nuclear Sciences and Physical Engineering, Department of Solid State Engineering
Academic year	2023
Number of pages	103
Keywords	thin films preparation, thin film characterization, Ionized Jet Deposition method, high temperature superconductors, scanning electron microscopy, X-ray diffraction

Abstrakt

Tato disertační práce se zabývá přípravou tenkých vrstev vysokoteplotních supravodičů s důrazem na studium vlivu depozičních parametrů metody Ionized Jet Deposition. Ionized Jet Deposition (IJD) je nová metoda přípravy tenkých vrstev využívající pulzní eletronový svazek k ablaci terčíku. Tuto metodu přípravy tenkých vrstev řadíme mezi metody fyzikální depozice z par. Mezi hlavní přednosti metody IJD patří její flexibilita spočívající v možnosti modifikovat proces nanášení pomocí širokého spektra depozičních parametrů. Mechanické vlastnosti vysokoteplotních supravodičů, především jejich značná křehkost, limitují jejich praktické využití. Proto je z technologického hlediska vhodné připravit je ve formě tenkých vrstev deponovaných na pružných substrátech a z nich poté sestavovat složitější struktury, jako např. vodiče elektrické energie.

Při podrobném studiu vlivu depozičních parametrů na přípravu tenkých filmů je třeba nejdříve popsat teoretické základy samotné metody a dále základní charakteristiky materiálů, které jsou předmětem práce. Tento teoretický úvod je obsahem první části této práce.

Druhá část práce je zaměřena na studium samotných depozičních parametrů, jmenovitě urychlovacího napětí, vzdálenosti mezi substrátem a terčíkem, hustoty a chemického složení terčíku, typu substrátu a teploty substrátu během depozice. Jako ideální hodnota urychlovacího napětí se ukázelo napětí 14 kV a vzdálenosti mezi substrátem a terčíkem 110 mm. Zkoumaná hustota terčíků se pohybovala v rozmezí $3,85\ g/cm^3$ až $5,6\ g/cm^3$. Hustota terčíků zásadně ovlivnila rychlost růstu vrstev, ale má minimální vliv na morphologii povrchu zkoumaných vrstev. Typ susbtrátu zásadně ovlivňuje vnitřní strukturu nanesených vrstev stejně jako teplota substrátu během depozice. Bylo nalezeno rozmezí teplot, při kterém dochází k žádoucímu uspořádní vnitřní struktury. Tato teplota je okolo $780°C$ při depozici vrstev na speciální páskový substrát vyvinutý pro přípravu vysokoteplotních supravodivých tenkých vrstev. K dosažení plně supravodivé vrstvy je ještě zapotřebí s největší pravděpodobností upravit chemické složení nanesených vrstev. Tato úprava může být provedena změnou chemického složení terčíku na základě transportních koeficientů zjištěných pomocí studia terčíků s různým složením a nebo zvýšením urychlovacího napětí což bude mít za výsledek zvýšení energie jednoho pulzu elektronů a tedy lepší zachování stechiometrie mezi terčíkem a deponovanou vrstvou.

Abstract

This dissertation deals with the preparation of thin films of high-temperature superconductors with emphasis on the study of the influence of deposition parameters of the Ionized Jet Deposition method. Ionized Jet Deposition (IJD) is a new method of thin film preparation that uses a pulsed electron beam to ablate the target. This method of preparation of thin films is classified as Physical Vapor Deposition. The main advantages of the IJD method include its flexibility in the possibility of modifying the deposition process using a wide range of deposition parameters, which in turn allows the preparation of layers from almost any material. The mechanical properties of high-temperature superconductors, especially their considerable fragility, limit their practical use. Therefore, from a technological point of view, it is advisable to prepare them in the form of thin layers deposited on flexible substrates and then assemble more complex structures from them, such as electrical power conductors.

In a detailed study of the influence of deposition parameters on the preparation of thin films, the theoretical foundations of the method itself must first be described, as well as the basic characteristics of the materials that are the subject of the work. This theoretical introduction is the content of the first part of this work.

The second part of the thesis is focused on the study of the deposition parameters themselves, namely the accelerating voltage, the distance between the substrate and the target, the density and chemical composition of the target, the type of substrate and the temperature of the substrate during deposition. The ideal value of the accelerating voltage turned out to be 14 kV and the distance between the substrate and the target was chosen 110 mm. The investigated target density ranged from 3.85 g/cm^3 to 5.6 g/cm^3. The density of the targets significantly affected the growth rate of the films, but it has a minimal effect on the surface morphology of the investigated layers. The type of substrate affects the internal structure of the deposited layers; the same holds for the temperature of the substrate during deposition. A temperature range has been found at which a suitable arrangement of the internal structure occurs. This temperature is about $780°C$ when depositing the films on a special tape substrate developed for the preparation of high temperature superconducting thin films. To achieve a fully superconducting film, it is still necessary to adjust the chemical composition of the prepared films. This adjustment can be done by changing the chemical composition of the target based on the transport coefficients found by studying targets with different composition or by increasing the accelerating voltage, which will result in increased energy of one electron pulse and thus better preservation of stoichiometry.

Acknowledgements

I would like to thank everyone who gave me any kind of support in any of my activities during the time when I was a Ph.D. student. Special thanks go to my parents who supported me throughout my long studies. I would also like to thank my wife for the support she gave me during my studies and for sticking with me until the end.

Our work related to the topic of this thesis was partially supported by the following projects:

Center for advanced applied science, grant no. $CZ.02.1.01/0.0/0.0/16_019/0000778$

Grant Agency of the Czech Technical University in Prague, grant no. $SGS22/183/OHK4/3T/14$

The Czech Science Foundation, grant no. $GA21-05259S$

Author’s declaration

I confirm having prepared the thesis by my own and having listed all used sources of information in the bibliography.

Prague, 13 april 2023 Jakub Skočdopole

Contents

1 Introduction **1**

1.1 Content of Thesis 2

1.2 Research Goals 3

1.3 Publication of Achieved Results 3

1.4 Challenges for Future Research 4

1.5 Consequences for Applications and for Future Development of Science 5

2 Theoretical Part **7**

2.1 Ionized Jet Deposition 8

2.2 Growth of Thin Films 21

2.3 Applied Analytic Methods 24

2.4 High Temperature Superconductors 32

3 Experimental **37**

3.1 Accelerating Voltage and Substrate Positioning 38

3.2 Target Density 40

3.3 Chemical Composition of Target 47

3.4 Characterization of Structural Properties of HTS Films 52

3.5 Characterization of Superconductive Properties 66

4 Conclusions **71**

List of abbreviations **74**

List of Figures **76**

List of Tables **80**

References **81**

1 Introduction

The research goal of this thesis is to elucidate a deposition processes using the ionized jet deposition (IJD) for preparation of High Temperature Superconductors (HTS) thin films. The reader will be acquainted with the procedure of step by step examination of the individual deposition parameters. These parameters are necessary to fully understand the complex problem of deposition process. For easier understanding of the topic, the first part of this thesis contains introduction to the theory describing in detail the applied method, IJD, main features of thin films growth by physical vapour deposition techniques, and basic specifics of the studied class of materials, high temperature superconductors. The second part of the thesis is then focused on the obtained results, providing the detail description of individual deposition experiments performed, characterization of the prepared structures and discussion of the collected findings.

1.1 Content of Thesis

The thesis is structured in the following way:

1. Chapter 1 The introduction of the thesis. Overview of the planned and achieved goals, reasons why to use IJD method for preparation of high temperature superconductors (HTS) thin film, and how the results obtained in this thesis can influence the future of industry and science.

2. Chapter 2 The theory of IJD, Thin film deposition and HTS. The section dealing with IJD method describes in detail physical principles and experimental setup of the method. In the next part, the basic theory of thin films growth process by PVD is given, accompanied by description of the experimental techniques used to characterize thin films. Finally, the section is closed by overview of the main features of HTS materials, in particular of these important from the point of thin films fabrication.

3. Chapter 3 Overview of the performed experiments, achieved results and their discussion. Investigation of the influence of different deposition parameters on the properties of the prepared thin films. The properties of films examined in detail involve their thickness, surface morphology, chemical composition, structure and superconductive behavior. The investigated and discussed deposition parameters cover accelerating voltage, substrate positioning, substrate temperature, target density and target chemical composition.

4. Chapter 4 The Conclusion contains detailed summary of all obtained results, and suggestions for the future research in this field.

This thesis was processed by the author using LaTeX. Technical drawings and visualisation of results in this thesis were created using *Origin* and *ImageJ*.

1.2 Research Goals

1. Creation of a general set of theoretical knowledge needed for IJD usage
2. Experimental examination of the influence of the chosen IJD deposition parameters on properties of prepared thin films
3. Development of IJD thin film deposition applicable to HTS

1.3 Publication of Achieved Results

Individual parts of the research contained in this Ph.D. thesis were published in impact journals and presented on international conferences. Some results were published in bachelor thesis performed under supervision of the author.

1. The Study of influence of target properties namely target density and target chemical stoichiometry was performed on series of samples. The examination was focused on attributes of the thin films such as thickness of the films, surface morphology and chemical composition of the films. Obtained results were presented on virtual conference *ASC* 2020 and published in the *IEEE Transactions on Applied Superconductivity*. [1] [2]
2. The Study of different substrate types influence on the YBCO thin films deposited by IJD was presented on the international conference *EUCAS* 2021 as a poster with name *Influence of the properties of HTS thin films prepared by IJD depending on the substrate type.*
3. Examination of substrate temperature dependence on the structural phase of prepared thin films was done by X-ray diffraction. It was proven that the phase transformation occurs around temperature $750°C$. Part of the research data is included in the bachelor thesis of Bc. Tibor Koštál [3] performed under supervision of the author. Obtained results were also presented on conference *ASC* 2022 and published in the *IEEE Transactions on Applied Superconductivity*. [4]

1.4 Challenges for Future Research

The technology of HTS superconducting films preparation is still far from completeness; there is much to do in order to further improve and simplify the deposition process, thus making the production of the devices utilizing these layers more efficient. The general points that might be improved, regardless the deposition method applied, involve:

1. Increasing the critical current I_c, which are the HTS thin films capable to withstand.
2. Preparation of buffer layers necessary for HTS thin film grow by IJD
3. Up-scaling the deposition process to industrial scale.
4. Development of complex process of multi layer deposition (buffer, HTS film and protecting layer) and post-deposition treatment performed in a single device in order to improve the efficiency of HTS thin films production.

Restring on IJD only, the most important and ultimate goal is a successful deposition of HTS layers showing superconducting properties at LN temperature. Aim of the presented thesis is to provide a valuable initial contribution to this effort.

1.5 Consequences for Applications and for Future Development of Science

High temperature superconductors have recently experienced a large increase in usability in practice. One large group of practical applications attracting a considerable attention recently focuses on the use of superconductors in devices exploiting effect of magnetic levitation. This phenomenon allows to contactless transmit motion, which can be applied in many ways. Currently, magnetic levitation is used, for example, in drug mixers, where non-contact motion transmission prevents contamination of the agitated substances with materials that may be present at the engine that drives the agitator. Furthermore, levitation conveyors are being developed, which can be crucial for objects transportation e.g. in high-risk areas [5]. The properties of superconducting magnetic levitation make it possible to move all control electronics and conveyor motors to a separate section, thus eliminating potential sources of danger. Other practically important property of any superconductor is the ability to shield/compensate the magnetic field, which is very crucial for highly sensitive measurements of magnetic fields of very low intensity. A superconducting quantum interference device (SQUID) is usually used for these measurements.

Ability of loss-free transmission of high electric currents belongs then to the main application domain of superconducting leads composed of laminated HTS thin films. All recently known HTS materials suitable for for application in cable construction belong to ceramics materials, showing thus very limited mechanical flexibility. Thus, it is necessary to construct the leads as multistrata assemblies composed of stack of flexible strips, each covered by a thin HTS layer. Technological progress has enabled the economically advantageous use of superconducting cables cooled by liquid nitrogen. The use of superconducting cables is particularly feasible over short distances and lower voltages, where electrical losses are the greatest. These cables also take up significantly less space than conventional copper conductors. The combination of these properties makes superconducting cables an ideal choice for the backbone of underground electrical networks in the cities or short distances between power plants and highly energy-intensive production places, such as an aluminum factory. HTS cables can also be used in electromagnets with the possibility of creating an extremely strong magnetic field. These strong magnetic fields are essential eg. for fusion power plants technologies such as ITER.

Theoretical Part 2

This chapter deals with three distinguished physical areas playing key role in the performed research. Knowledge of these subjects is necessary in order to understand the complex issues of high temperature superconductor thin film preparation by IJD method. The first subsection is focused on the IJD deposition method itself. Description of the method is divided in two parts, the detail explanation of the deposition process, and the description of particular parameters influence. The second section is focused on processes accompanying growth of thin films. The last, third section then introduces the class of materials denoted as high temperature superconductors (HTS).

2.1 Ionized Jet Deposition

The resulting properties of the thin films prepared by different deposition techniques are influenced by many different aspects. Each deposition technique have its unique set of deposition parameters which define capability of the given method to prepare thin films of particular type and composition. In this section, the IJD deposition parameters are introduced, with closer attention given to acceleration voltage, distance between target and substrate, substrate temperature and target properties (density, heat conductivity and chemical composition).

The rest of the deposition parameters, which are monitored during each deposition process performed by IJD includes deposition time, frequency of electron beam pulses, working gas, type of substrate, cleaning pressure, working pressure and distance between the target surface and the bottom of equipotential space/flight-trough cathode.

The Ionized Jet Deposition method was developed during the last decade by the team of Italian company Noivion srl. The IJD is a physical vapor deposition method which uses a special configuration of pulsed electron beam for target ablation. Novelty of this methods requires a complex approach to development of brand new deposition processes. This is also the case of the deposition process aimed on preparation of high temperature superconductors thin films. It is worth to notice that the IJD method has some common attributes with other deposition techniques, such as pulse laser deposition, magnetron sputtering and mainly channel spark deposition. Information from deposition processes prepared for these methods has been used as the basis in creating the deposition process for IJD.

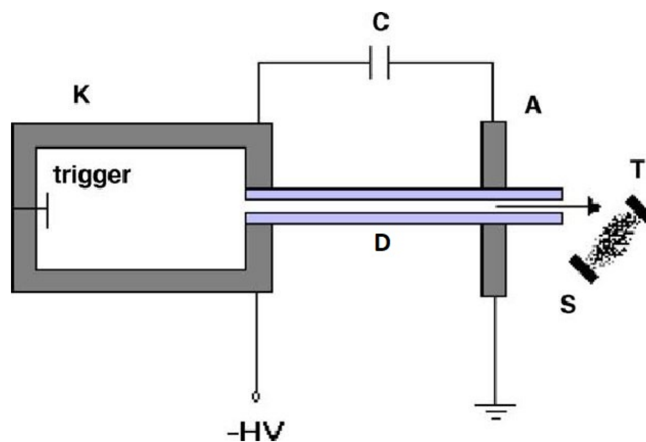

Figure 2.1: Schematic of channel-spark electron beam source; in the picture, K marks the hollow cathode, A - anode, C - capacitor, HV - the negative port of high voltage generator, T - target, S - substrate, and D - dielectric tube. [6]

The IJD method is a direct successor of so-called channel spark deposition method. Schema

of the latter is shown in Fig. 2.1 Channel spark method also uses pulsed electron ablation to vaporize the target [7]. However, the overall design of the two methods differs, and, in case of IJD, it is optimized to achieve better deposition and utility properties. The main difference consists in the displacement of the hollow cathode which serves as the main source of electrons needed for target ablation. In the case of IJD, this cathode is moved in a close vicinity of the target, the arrangement thus minimizing undesired energy losses 2.2. Also, placing the cathode close to the target eliminates the need of using dielectric tube, which serves in the channel spark deposition as the electron supply channel to the target. This supply tube has to be frequently replaced after certain deposition time due to its clogging with the deposited material. Overall, IJD offers a more mechanically robust system that provides a better deposition performance than the channel spark deposition due to the improved system geometry. The higher deposition performance in this context means the better energy transfer between the deposition system and the target which results in a faster and more controllable process of thin films preparation.

2.1.1 IJD Deposition Process

The key working tool of IJD method is the pulsed electron beam generated in the IJD source (Fig. 2.2). The whole IJD source is located in vacuum chamber and operates at the pressure between 10^{-4} $mbar$ and 10^{-3} $mbar$ kept inside the vacuum chamber. During the deposition, the pressure inside the source itself is around 1 $mbar$. As shown in Fig. 2.2, the selected working gas is flowing trough the source from the right side, from the gas inlet, to the deposition target located at the left side of the picture.

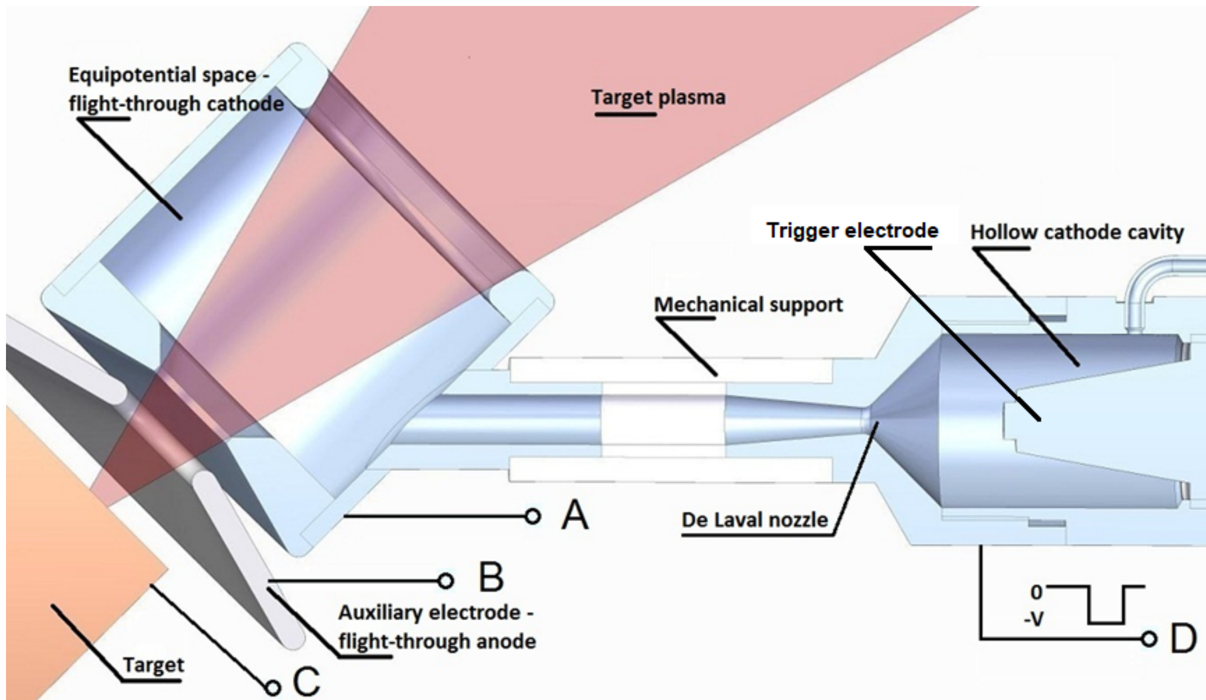

Figure 2.2: Schematic view of IJD source [8]; the letters A,B,C and D indicate electrical connections (B, D) and groundings (A, C)

The electric arc ignited in the hollow cathode cavity between the trigger electrode located in the center and the wall creates the primary electrons. The hollow cathode cavity wall and the equipotential space/flight-trough cathode (shown on left side of Fig.2.2) are both set at a high negative potential($-10kV$ to $-25kV$). The trigger electrode in the hollow cathode cavity is gradually brought to the ground potential. This potential change is done by suitable resistors. The electric arc is ignited when the potential difference between the trigger electrode and the outer wall is over the break down voltage of the flowing gas mixture.

The primary plasma created in the hollow cathode cavity is kept at a slightly higher positive potential than the equipotential space/flight-trough cathode wall. This potential difference is controlled by the positive potential of the trigger electrode in the hollow cathode cavity. The

produced plasma then propagates and expands toward the equipotential space/flight-trough cathode by passing the intermediate De Laval nozzle. The latter creates a laminar flow of the working gas ionized by the primary electrons during their propagation toward the equipotential space/flight-trough cathode. The positively charged ions from the working gas effectively shield electrons in the plasma, allowing thus to increase the electric current density compared to other methods, using electron beams in vacuum. The increase is from mA up to kA. The laminar flow of working gas ions also drags surroundings electrons, effectively acting as a pinning done by magnetic field used in channel spark deposition method.

When the plasma arrives into the equipotential space/flight-trough cathode the latter starts to behave as an ordinary hollow cathode [9] (Fig.2.3). Electrons start to oscillate between the walls and the cathode axis, where the potential level is more positive due to the spacial expansion of the anode potential in to the cathode volume. In this situation, the grounded target acts as a positively charged anode. The oscillation of electrons starts to create secondary electrons by avalanche ionization of the working gas. When the overall amount of electrons generated by the hollow cathode effect increases enough, an arc toward the target is ignited, in accordance with the Paschen law (Fig. 2.4).

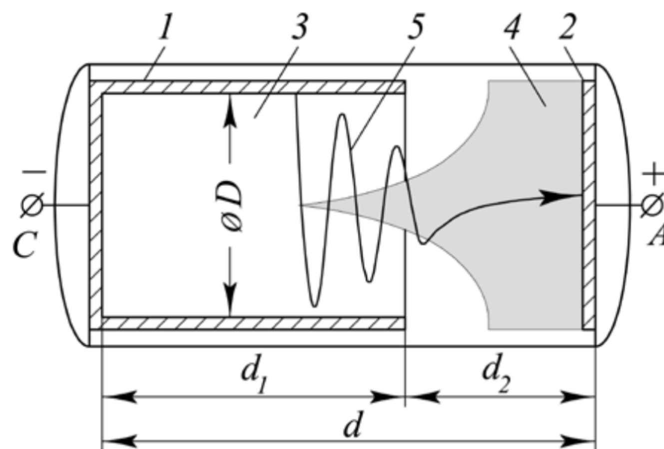

Figure 2.3: Schematics of hollow cathode effect; 1-hollow cathode, 2-grounded anode, 3- area of positive charge near the walls, 4-plasma channel, 5-electron trajectory, A,C-electric connections, D-diameter of the hollow cathode, d1,d2,d-characteristic distances [9]

The Paschen law describes the dependence of breakdown voltage on the pressure and distance between two electrodes (Rel. 2.1). The IJD source operates generally at the pressures corresponding to the left side of the Paschen curve with respect to the minimum of the curve shown in Fig. 2.4).

$$V = \frac{aPd}{\ln(bPd)} \tag{2.1}$$

Here V is the breakdown voltage $[V]$, P is the pressure $[bar]$, d is the distance between electrodes $[mm]$ and a and b are constants reflecting the actual gas composition [10]. In case of ambient air, the constants are $a = 43.6 * 10^6[V/(bar * m)]$ and $b = 3.62 * 10^5[1/(bar * m)]$. For IJD system, the typical pressure $P = 1 * 10^{-3}[bar]$ and the distance between the equipotential space/flight-trough cathode and the target (which are the Paschen electrodes in this system) is $d = 3 * 10^{-3}[m]$. After substituting these values into the equation 2.1, the IJD breaking voltage $V \approx 18[kV]$ is obtained. This value is in a good agreement with the voltage values measured on a real IJD system. Table 2.1 then gives summary of other key parameters characterizing typical IJD pulsing source [11].

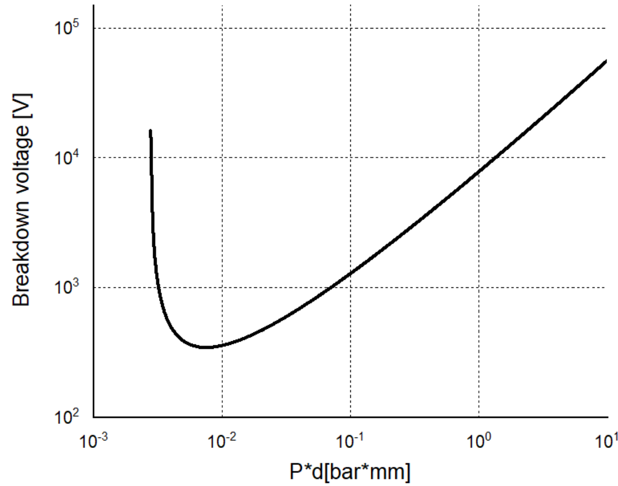

Figure 2.4: Paschen curve (calculated after Rel. 2.1) providing dependence of the breakdown voltage on the product of pressure and distance [10]

The arc creates a conductive plasma channel towards the target, however, if a source (in this case an IJD source) is connected to the circuit providing such an amount of electrons that it exceeds the capacity of the plasma channel, a charge double layer will form [12]. The charged

Table 2.1: Characteristic IJD pulse parameters (unpublished data Noivion srl. and [11])

Discharge voltage	$30kV$
Electric efficiency	30%
Gas pressure	$1 * 10^{-3} mbar$
Discharge time	$200 - 1000ns$
Frequency of pulses	$5 - 600Hz$
Maximal electron energy in the beam	$\leq 15keV$
Total electron current	$\leq 3.5kA$
beam diameter at target	$0.5 - 2mm$
Current density	$\leq 10^5 A/cm^2$
Power in the beam	$\leq 440MW$
Power density in the beam	$\leq 14MW/cm^2$

double layer is in balance with the difference in electrical potential inside the plasma (Fig. 2.5), such situation can be achieved when the mobility of electrons is higher inside the plasma channel than in the rest of the electric circuit, and when the electric charge capacity of the plasma channel is exceeded. Thus, as a result, in one side of the channel a surplus of electrons, and on the other side their shortage appears, the situation which effectively creates an electric potential. This potential difference increases the energy of electron beam accelerated toward the target surface and causing its ablation.

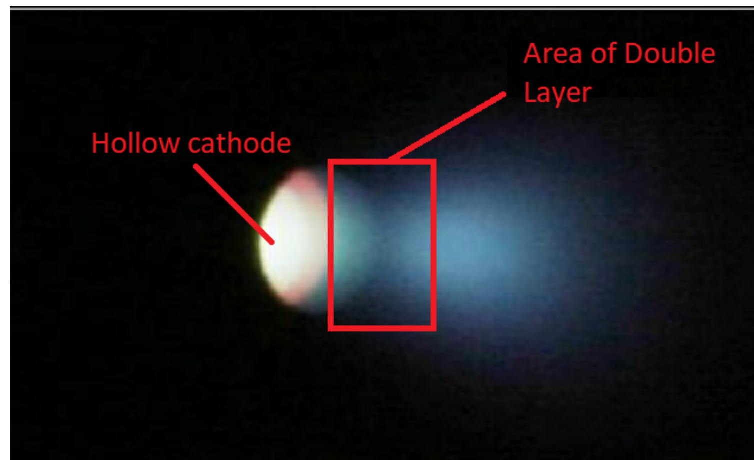

Figure 2.5: Picture of the double layer emitted from the hollow cathode; the negative charge region appears darker than the positive charge ones, due to the greater emission of light photons by positive ions comparing the photon emission from the negative electronic cloud [13]

The plasma of the target material created by the ablation then expands trough the equipotential space/flight-trough cathode. There are two openings in the cathode. One is in the bottom part, facing the target and the second one in the top part facing the substrate. These two openings in the cathode are used to produce a cone-shaped plasma plume with the apex angle ca. 30° (Fig. 2.6). Within this cone, the plasma plume should be highly homogeneous, without clusters created during the ablation process on the surface of the target. These clusters are mostly solid particles ripped from the target.

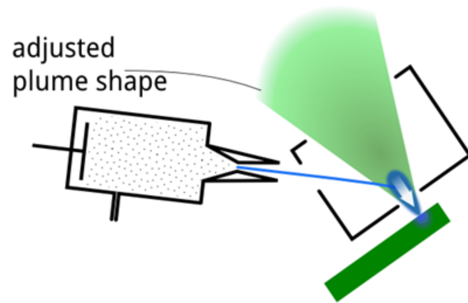

Figure 2.6: Schematic of the plasma plume ablated by the IJD source from the target (green)[8]

2.1.2 Ablation Process

The term "ablation" means generally a removal of something by its vaporization. In case of thin film deposition methods, the ablation of the target material in explosion-like manner, by a source generated particles with sufficient energy. These particles are ions in the case of magnetron sputtering, photons for pulse laser deposition, or electrons when a pulse electron source is used. Further on, we will focus only on ablation of material by means of pulsed electron beams. For the electron beam ablation, the energy of incoming electrons is crucial, since it has a strong influence on the penetration depth of electrons in the target material. For electrons within the energy range $1keV \leq E \leq 20MeV$, the penetration depth δ $[\mu m]$ can be calculated using the approximation [14]

$$\delta \approx 5.37E\left(1 - \frac{0.9815}{1 + 0.0031E}\right)\frac{1}{\rho} \tag{2.2}$$

Here ρ $[g/cm^3]$ is the target mass density, and E $[eV]$ is the energy of the incident electron beam.

The physical mechanisms influencing the actual penetration depth value involve mainly Coulombic interactions, inelastic electron scattering on ionic cores and emission of secondary electrons and photons. A part of incident electrons can be also elastically/inelastically reflected. The probability for Coulomb scattering to occur is very large. Due to the Coulomb scattering, the electrons interact with the solid material in a zigzag manner, and the energy transfer to the target is not uniformly distributed along the entire penetration depth. The total power absorption per unit volume of the target ($P_{max}[W/cm^3]$) and its spacial dependence $P(z)$ can be approximated by the relations 2.3 and 2.4 derived in [15].

$$P_{max} = \frac{4}{3}(1-k)U\frac{j}{\delta} \tag{2.3}$$

$$\frac{P(z)}{P_{max}} = 1 - \frac{9}{4}\left(\frac{z}{\delta} - \frac{1}{3}\right)^2 \tag{2.4}$$

Here j $[A/cm^2]$ is the electron beam current density, z is the depth in the target along its surface normal, U $[eV]$ is the electron beam energy and k is the reflection coefficient. The normalized power absorption course calculated using the relations 2.3 and 2.4 is shown in Fig. 2.7.

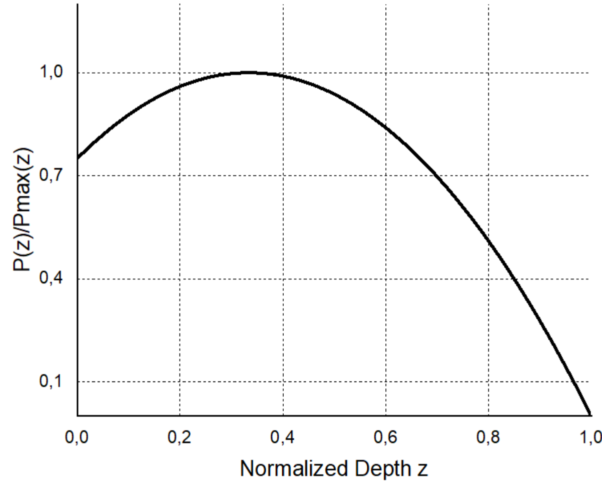

Figure 2.7: Normalised absorbed power of electron beam along the depth below the target surface z [11]

The target material is vaporized anywhere along the beam path where the absorbed specific energy exceeds, or is equal to the evaporation heat. This process is heavily influenced by the thermal conductivity of the target. A lower thermal conductivity of the material can help concentrate enough absorbed energy at one spot, sufficient to overcome the evaporation threshold before the energy is relaxed away in form of heat. Thus, a prevailing part of the energy loses occurring during the ablation process is due to the heat flow in the bulk increased further by the energy absorbed at the locations where the evaporation thresholds is not reached.

The electron beam carries a minimal momentum but a lot of energy to the target, making possible the ablated material to leave the target surface along the normal direction to the surface. The angular distribution of the material measured in ref. [11] approximately follows the distribution $cos^{2.5}(\alpha)$ where α denotes the emission angle with respect to the surface normal (Fig. 2.8).

This incident material distribution results in the growing film thickness distribution on to the substrate to be proportional to the $cos^{5.5}(\alpha)$. As mentioned in the previous section, the IJD method uses plasma plume with the apex angle ca. of 30° which guarantees the film thickness deviations lesser than 10% (Fig. 2.9).

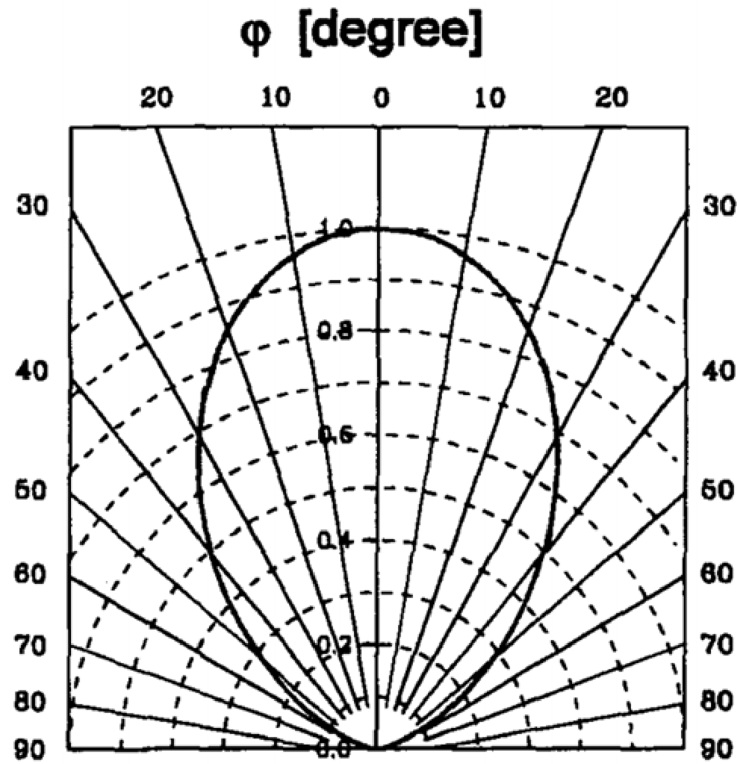

Figure 2.8: Normalized angular distribution of target material ablated by IJD source [11]

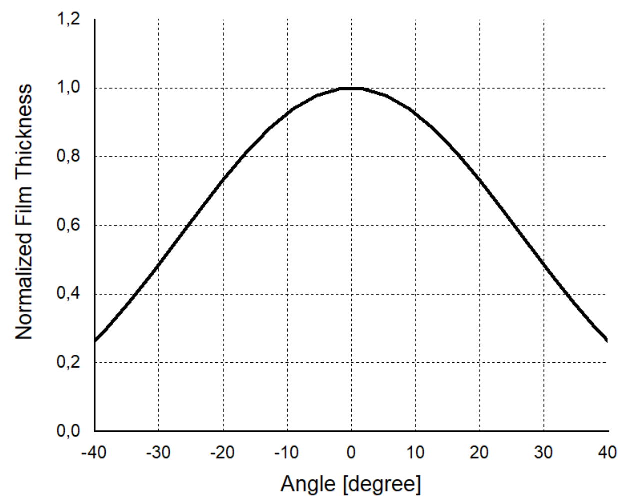

Figure 2.9: The typical normalized distribution of the growing film thickness as function of the deviation from the IJD plasma plume axis (typically parallel to the sample surface normal) [11]

2.1.3 Plasma Plume Propagation Between Target and Substrate

Plasma created during the ablation process is the main source of material for the growing thin film. The plasma plume is propagating along the direction perpendicular to the target surface. Since ions in plasma undergo several energetic changes during their travel from target to the substrate, the plasma propagation can be divided into the following four stages [16] (Fig. 2.10).

The first stage consists in creation of the plasma plume during the ablation process itself. Duration of this phase is governed by duration of the electron pulse. The energy of electrons is transformed into the internal energy of plasma. The height of the plasma plume during this phase is typically under 1 mm .

During the second phase of plasma propagation toward the substrate, most of the plasma is ejected along the target surface normal. The exact direction of the plasma expansion in governed by its internal pressure. Since the generated plasma is created inside the target bulk, the only direction along which it can expand is close to the direction opposite to the incoming electron beam. From other sides the expanding plasma is bounded by the target mass. These conditions result in the ejection of plasma perpendicular to the target surface. Moreover, the density of plasma is much higher than the density of the residual gas in the chamber, and the ejection process is thus not affected by the surrounding atmosphere influence. The distance which plasma travels in this phase is around 10 mm.

In the third phase, the atoms and ions in plasma start to collide with atoms of the background/working gas. As a result, the energy of plasma starts to change, the latter effect influencing the mean free path of the carried particles. The ablated atoms create, trough mutual interactions with the gas atoms, the so-called "snowplow effect" resulting in dragging the gas atoms towards the substrate. This effect may be important during a reactive deposition when the plasma atoms chemically react with the working gas atoms to create the desired chemical composition of the growing film. Preparation of titanium nitride from a pure titanium target and nitrogen used as the working gas can serve as an example. During this phase, the plasma and the dragged atoms decelerate, and decrease their kinetic energy. The expansion of plasma propagation reaches distance around 100 mm from the surface of the target.

The last phase occurs when the directional velocity of the plasma plume is comparable with the thermal velocity of its constituting atoms. The expansion of the plasma plume almost stops. For a standard deposition process, the distance the plasma plume reached (marked further on as L_0) is the ideal position where the substrate should be placed [16]. The theoretical model

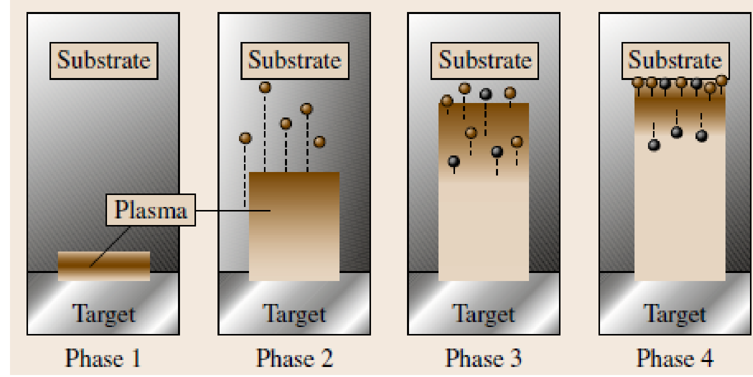

Figure 2.10: The four phases of plasma plume propagation described in text [16]

proposed in Ref. [17] can be used for finding this location. The model treats the ablation process as the adiabatic one. N_0 atoms is ablated per unite time and volume, with the initial average velocity v_0 and scaling distance L_0 considered as function of the particular ablation process and gas atmosphere parameters. The main phenomena elucidated in this model is the transfer of kinetic energy from ablated atoms to the thermal energy of plasma mixed with working gas particles. During the process, the total momentum and energy is assumed to be conserved. As the result, the directional particle velocity v and the thermal velocity v_T can be estimated and calculated following the relations 2.5 and 2.6 (For more details of the model see Ref. [17]).

$$\frac{v}{v_0} = (1 + x^3)^{-1} \tag{2.5}$$

$$\frac{v_T}{v_0} = x^{3/2}[3(1 + x^3)(1 + \mu x^3)]^{-1/2} \tag{2.6}$$

Here, $\mu = M/m$ is the atomic mass ration between the target material and the gas particles and $x = L/R$ is the normalized propagating distance. The symbol R marks the distance where the moving set of particles consists of equal mass of gas atoms and target material atoms. The intersection of the velocity functions $v(x)$ and $v_T(x)$ defines the location where the thermal velocity and the directional velocity of the plasma are equal to each other, thus providing estimate to the distance L_0 (Fig. 2.11). Usually however, this location is found and verified experimentally. It is safe to assume that the distance L_0 is the location where the most homogeneous thin films are grown. Said homogeneity is achieved due to the ideal energy level of the arriving particles, which is not to high to cause the film damages, but also sufficient for non-thermal activation of the substrate surface [16].

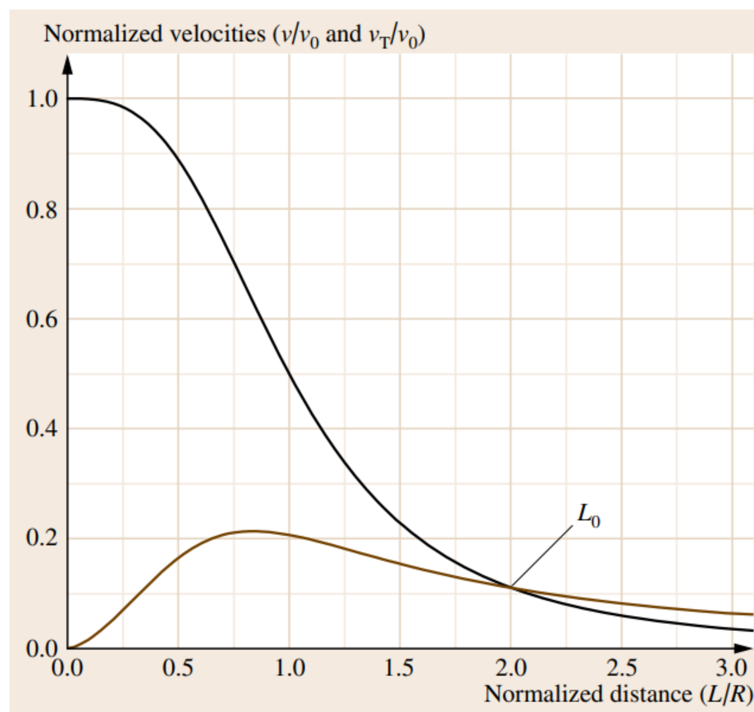

Figure 2.11: Graph of directional velocity v and thermal velocity v_T in dependence on normalized distance; the value L_0 is given by the intersection of both velocity curves [16]

2.2 Growth of Thin Films

This section aims to provide description of processes taking place in growth of thin films by PVD methods, with the particular reference to the IJD technique.

The thin film growth process starts when the plasma arrives at the substrate surface. The deposition and redistribution of atoms from plasma on the substrate surface is governed by set of physical and chemical parameters. Deposition of thin films by physical vapor deposition can be considered as a highly non-equilibrium process. The real structure of prepared thin films is a metastable state, thus the structure is easily changeable by exposition to additional energy. In general, the thin film growth process can by described as driven by kinetics of adsorption and diffusion, and divided into the following three subsequent parts. The first one is the nucleation, the second one is the coalescence and the last one is the voluminous growth [18].

The nucleation is a heterogeneous process of assisted condensation of the arriving plasma atoms on the substrate. For the nucleation process to start, it is necessary to achieve a supersaturation state $S > 1$, with the saturation level S defined as

$$S = p/p_0 \tag{2.7}$$

where p is the partial pressure of the arriving plasma and p_0 is the equilibrium vapor pressure at the substrate surface. The pressure of the arriving plasma can be deduced from the deposition rate R using the following relation.

$$R = p/(2\pi m K T)^{1/2} \tag{2.8}$$

where K is the Boltzmann constant, m is the molecular weight of deposited material and T is temperature of plasma.

The nucleation can lead to the three growth modes. These growth modes differ in the interaction energies between the arriving particles and atoms forming the substrate surface. Systematic division of the growth modes can be derived using Young´s equation represented by Rel. 2.9. The equation describes ability of liquid to maintain a particular contact angle with a solid surface in terms of surface specific energies of the involved phases expressed in terms of their inter-facial surface tensions.

$$\gamma_B = \gamma^* + \gamma_A \cos\varphi \tag{2.9}$$

where φ is the wetting (contact) angle, γ_B is the surface tension of the substrate, γ_A is surface tension of the growing film material and γ^* is the inter-facial tension between the film and the substrate (Fig. 2.12).

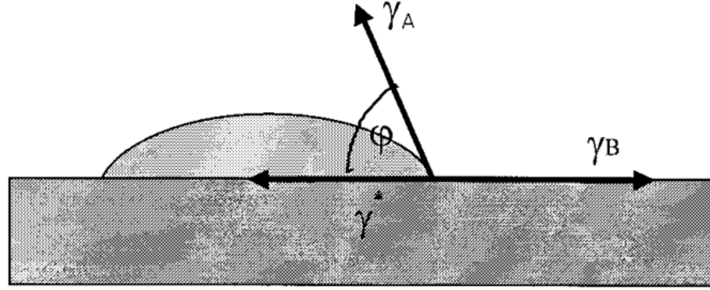

Figure 2.12: Scheme of the surface tension components acting at the growing film interface [19]

The island growth ($\varphi > 0$), called also as Volmer-Weber growth mode, requires $\gamma_B < \gamma_A + \gamma^*$. Overall contribution to the total free energy of the growing system due to the interaction between the growing film and the substrate is higher than the contribution from the free substrate and growing film surface. Thus, separated three-dimensional islands grow on the surface of the substrate.

The opposite case layer by layer growth ($\varphi = 0$), called also as Frank-van der Merwe growth mode requires $\gamma_B > \gamma_A + \gamma^*$. Interaction of the film and the substrate is energetically more favourable than the sum of the interactions between the film and substrate surfaces and the surrounding gas. Thus, regular layers of the film material grow on top of another.

Finally, the layer plus island growth called also as Stranski-Krastanov growth mode occurs when (in an ideal case) the first grown layer satisfies the condition for the Frank-van den Merwe growth mode, but the second and all other atomic layers of the growing film are conformal with the Volmer-Weber process. Growth starts as layer by layer growth and, with the increasing thickness of the film, changes to the island growth (Fig. 2.13).

The next stage of thin film growth process is the coalescence. At this stage, the nucleation centers fuse together. After solid-like coalescence of two nucleation centers, a grain boundary is created; after a liquidlike coalescence, a new uniform and boundary-free nucleation center is formed. End of this stage is defined by the percolation thickness threshold. The percolation thickness is the minimal thickness needed for the material to fuse together all the nucleation centers and to create a uniform macroscopic thin film. For most materials, this thickness is between $1nm$ and $20nm$.

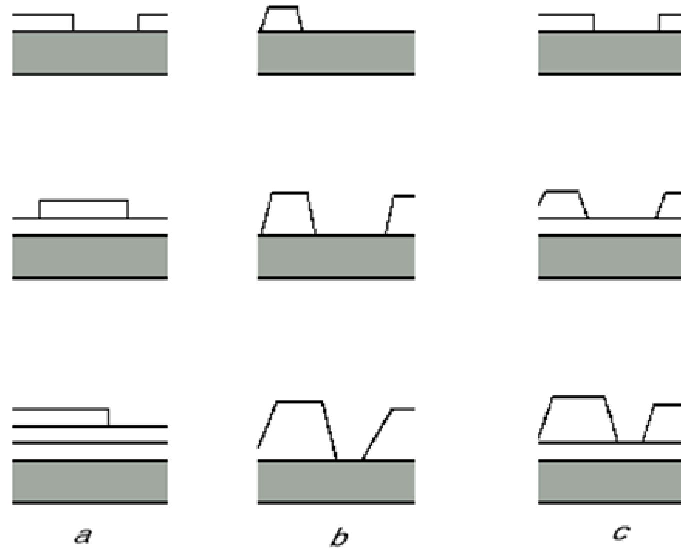

Figure 2.13: Schematic picture of the growth modes of thin films: Frank-van der Merwe mode (a), Volmer-Weber mode (b) and Stranski-Krastanov mode (c) [18]

For most applications however, the thickness of $20nm$ is not sufficient. Thus, the voluminous growth stage is needed, which is the last stage of thin films growth process. The complete real structure formation is then controlled mainly by the following processes.

Shadowing occurs when the arriving plasma flow shows a directional character. It dominates at low substrate temperatures, and geometric interaction of the arriving atoms and surface roughness of the growing film plays the key role.

Diffusion in this stage can be understood as a mobility of atoms on the substrate surface. For most materials, the diffusion is related to their melting temperature T_m. The diffusion can be separated onto the three different zones, depending on the ratio between the substrate actual temperature T_s and the melting temperature T_m of the growing film material. The first zone, for which holds $T_s/T_m < 0.3$, shows a low mobility of the incoming atoms. Thus, the atoms stay mostly at the positions where they land. In the second zone, with $0.3 < T_s/T_m < 0.5$, a surface diffusion occurs with the activation energies between $0.1 - 0.3$ eV resulting in a columnar real structure. In the last third zone, where $T_s/T_m > 0.5$, bulk diffusion dominates, with the activation energies above 0.3 eV resulting in an evenly grained real structure.

The last process of the growing sequence which affects the resulting real structure is recrystallization. The recrystallization takes place in films of larger thickness at substrates kept at high enough temperature during the deposition. Phase transitions and orientation changes may occur in such case[19].

2.3 Applied Analytic Methods

Analysis of thin films is a complex task. Many of the bulk analysis methods are not suitable for thin films examination. In this section, several methods are introduced which are used in this thesis. It is apparent that a careful and detail analysis of the thin films prepared from HTS materials is crucial for subsequent formulation of correct technological procedure leading to films with micro-structure showing the desired superconducting properties. Such analysis must be capable to elucidate the following four main properties: film thickness, surface morphology, chemical composition and crystalline structure. Thickness, as the basic parameter important for majority of thin films; surface morphology, since the HTS films are commonly overlaid by further layers in order to prevent damaging from exterior conditions, and character of the HTS film surface plays important role in preparation of such covering layers; chemical composition as being crucial for growth of the desired superconducting phase (for similar chemical stoichiometries, there are many chemically alike phases, but without superconducting behavior). The last critical property is the type of crystalline structure. It is highly influenced by the temperature regime during the deposition. Even with the correct chemical composition, it is necessary to find out the right temperature window for the film preparation in order to achieve the presence of superconducting phase. To obtain information about the upper mentioned properties, the below listed and briefly described methods have been used.

Scanning Electron Microscopy

The scanning electron microscopy (SEM) is an analytical imaging method based on scanning the sample surface with a focused electron beam and reconstructing the surface morphology from the recorded intensity of electrons released from the surface (Fig. 2.16). The primary electrons interact with the surface and underlying mass of the examined sample. Since the mean free path of low energy secondary electrons is short, only electrons released from few nanometers below the surface are detected, and used to reconstruct the surface topology image. This low depth of analysis is especially important for examination of thin films, because the undesired interference with the signal from the underlying substrate is depressed. In the particular case of the films prepared by IJD method, the SEM allows examination of typical surface morphology features, namely the number and size of "droplets" (Fig.2.14).

The SEM method can be also used for examination of the film thickness by scanning the section of the tested sample where it is possible to distinguish between the substrate and the

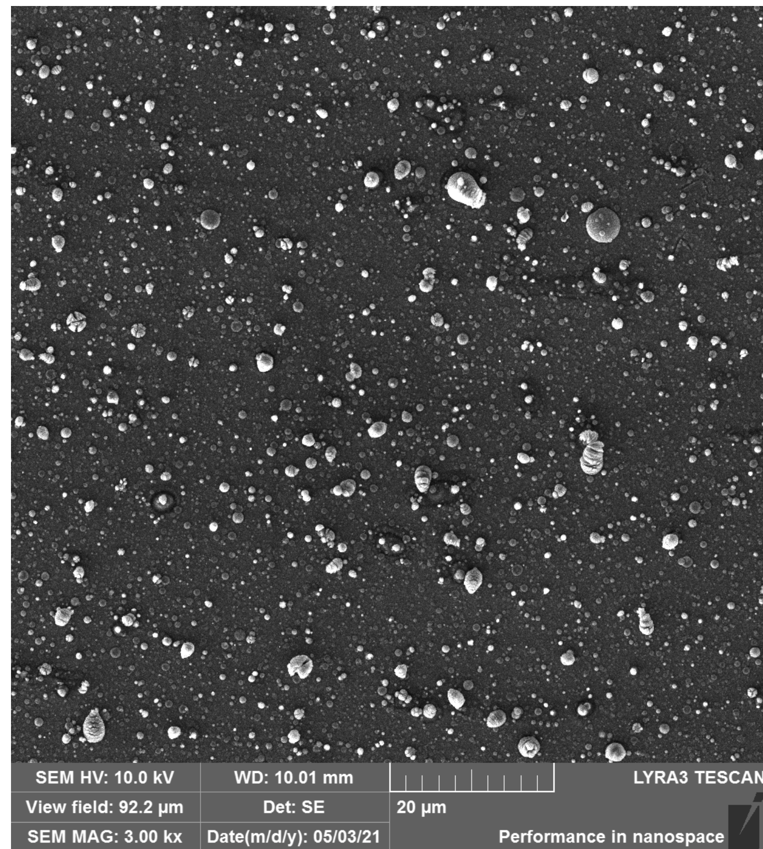

Figure 2.14: SEM image of YBCO thin film prepared by IJD method; "droplets" are clearly visible

deposited thin film. Orientation of such sample section plane has to be perfectly perpendicular to the primary beam of electrons. The latter setting is not always possible due to the sample holder or due to the geometry of the fracture. In latter cases, the obtained thickness is only approximate one, since it is not possible to precisely distinguish between the interior of the film fracture and the area belonging already to the surface of the film, visible due to the tilt of the sample (Fig.2.15) [8] [20].

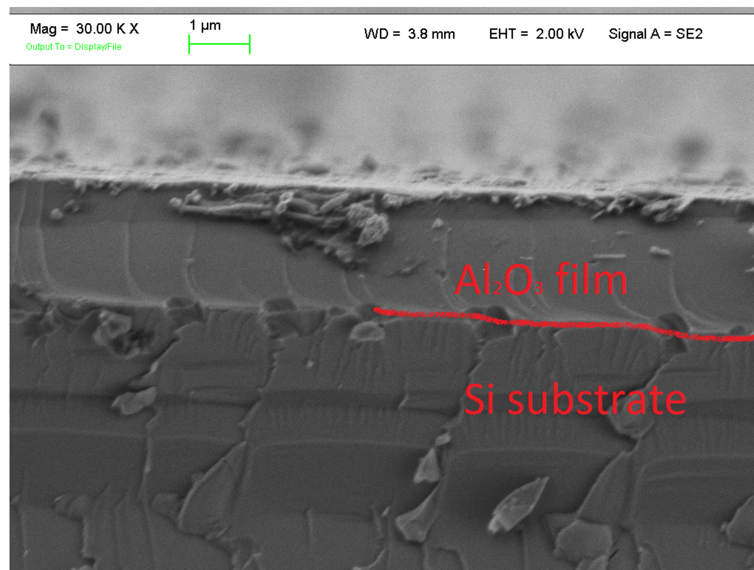

Figure 2.15: SEM micrograph of the fracture of Al_2O_3 thin film deposited on monocrystalline silicon wafer; the regions belonging respectively to the film and the substrate are indicated

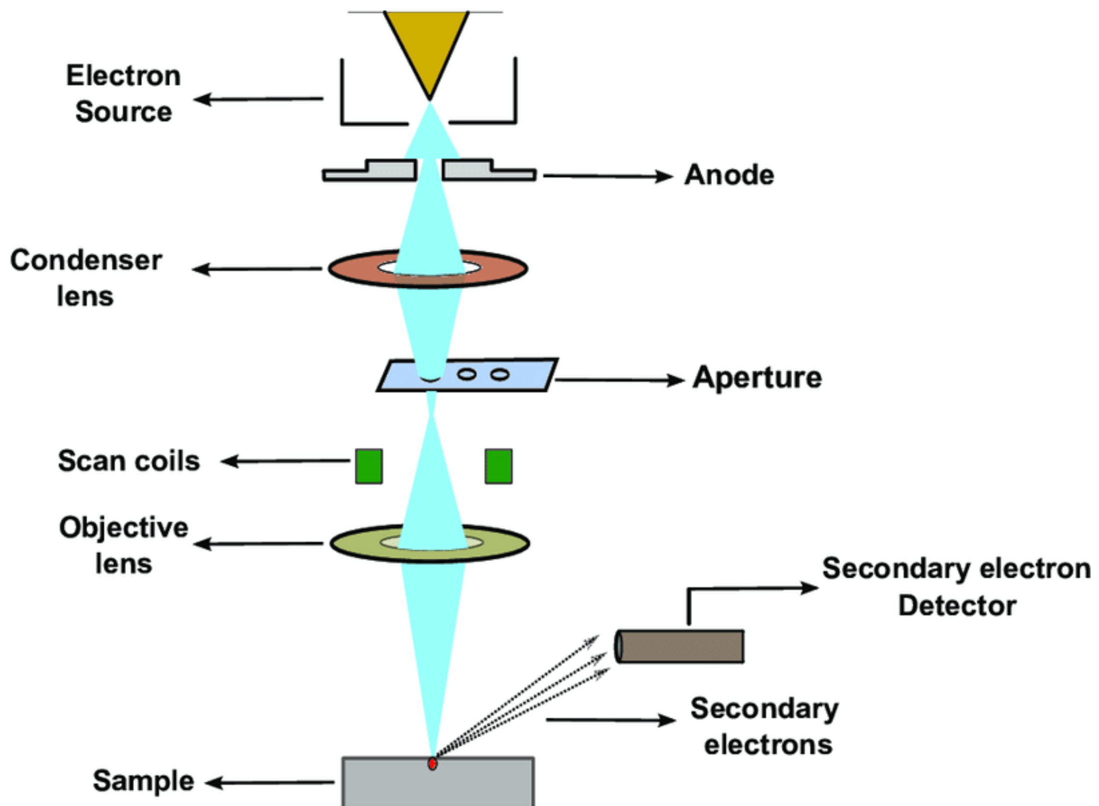

Figure 2.16: Schematic of SEM; in addition to the secondary electrons detector, an X-ray detector can be used too, providing EDS analysis [20]

Energy Dispersive X-ray Spectroscopy

The primary beam of electrons used in SEM initiates also some other distinguished types of interactions, resulting in emission of, e.g., Auger electrons, back scattered electrons and characteristic X-rays (Fig.2.17). Energy analysis of the latter forms a base of the method of energy dispersive X-ray spectroscopy (EDS). Schematic view of the EDS setup is shown in Fig. 2.16. Due to its unique electronic structure, each element has a unique spectrum of the emitted characteristic photons. Thus, the emitted characteristic X-rays can be used for qualitative as well as quantitative determination of chemical composition. Although the particular energies of the characteristic X-ray lines differ for different elements, the mean penetration depth of the emitted radiation is in the micrometer range. This poses a problem for thin film analysis, because there is high a interference with the signal from the substrate. To minimalize the latter effect, it is desirable to use substrate that contains completely different elements than the tested film. Thus, the EDS method can be effectively used for examination of the chemical composition of thin film when the film is thick enough to eliminate the signals from the substrate or if the substrate does not contain any of the chemical elements contained in the prepared film [21].

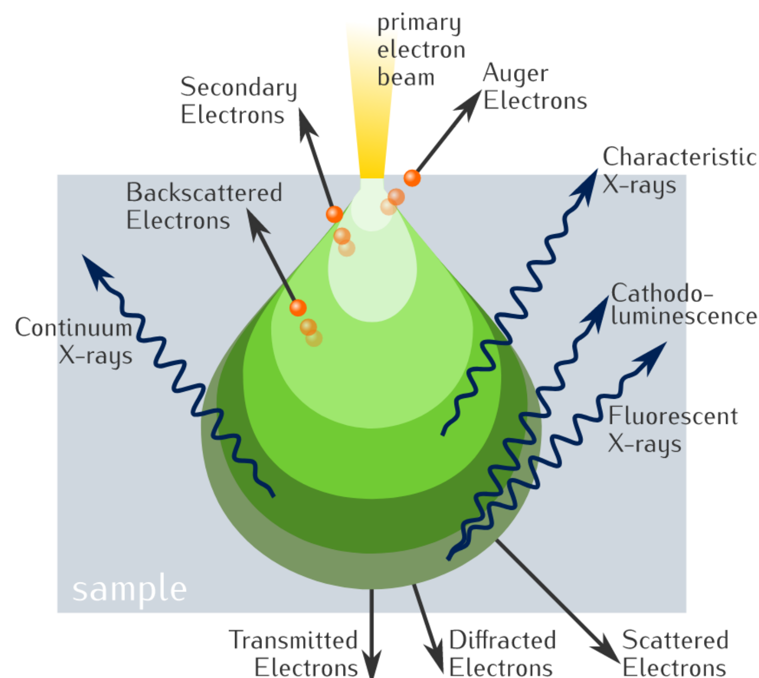

Figure 2.17: Scheme of interaction of primary electron beam with a solid sample [20]

Atomic Force Microscopy

The atomic force microscopy (AFM) is a useful tool for performing investigation of surface topology. The standard lateral as well as height resolution of AFM is in the order of nm. The surface is scanned by a mechanical probe. The probe consists of a tip which is mounted onto a set of piezoelectric translators. The tip "touches" or "feels" the surface and the bending of the tip that corresponds to the "landscape" of the surface is captured by the detection system. Typically, an optical reflection setup is used (Fig.2.18) or, nowadays, Akiyama probe which directly converts its bend into electrical signal. The AFM can be also used for film thickness measurement. For such measurement, it is necessary to create a step from the pure substrate to the thin film surface. The AFM scan running over the step then directly shows the film thickness [22].

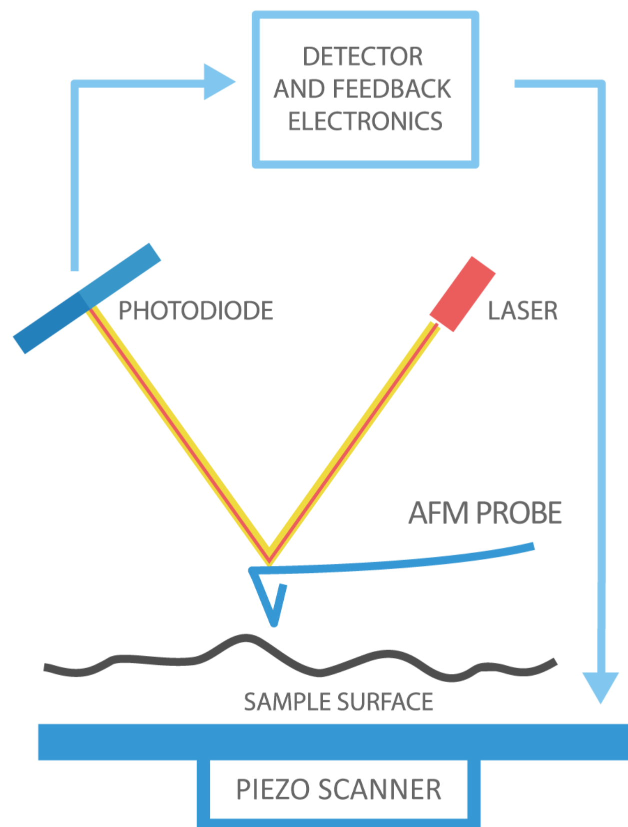

Figure 2.18: Schematic of AFM measurement with optical detection of the cantilever bend [23]

X-ray Diffraction

The X-ray diffraction (XRD) is a powerful analytical, nondestructive method for examination of inner structure of materials. As already mentioned, the penetration depth of X-rays reaches unites or even tens of microns, the value which seems to be large for analysis of sub micron thin films. To lower the penetration depth of the incoming X-rays, a techniques called grazing incidence angle scattering is used (Fig.2.19). In this setup, the primary beam of X-rays have fixed incidence angle ω $2° - 5°$ to the sample plain and the detector is scanning the range of diffraction angle (2θ). With this low incidence angle setting, the spot of the incoming X-ray beam on to the sample is highly prolonged. Information from a large volume of the thin film is obtained but, on the other hand, the sample has to be large enough to cover the whole spot of the beam. The X-ray diffraction can be also used for examination of the thickness of the thin film. There are two methods how the thickness can be obtained. The first approach is to analyse the reduction of the intensities of the diffraction peaks from the substrate. To be able to use this approach, it is necessary to have a diffraction record from the bare substrate, without the film present. In an ideal situation, a calibration standard sample with the film of the known thickness is used in addition. The second possibility how to measure the thickness by the X-rays is trough utilization of interference effect. At extremely low incidence angles, part of the X-rays is reflected from the surface of the film and another part is reflected from the interface between the film and the substrate. From the interference patterns of these two X-ray beams, the film thickness can be calculated according to the equation for position of the corresponding progressive interference maximum (2.10). This method is mainly used for the films with thickness in range of tens of nm [24] [25] [26].

$$2nd\cos(\theta) = (2k-1)\frac{\lambda}{2} \tag{2.10}$$

Here n is the refractive index of the film at the given wavelength, d is the sought thickness, θ is the angle of incidence of the wave on the film/substrate boundary, k is the order of interference maximum and λ is the wavelength of the x-ray beam.

X-ray Photoelectron Spectroscopy

The X-ray photoelectron spectroscopy (XPS) is a nondestructive analytic method used for determination of surface chemical composition. The XPS uses primary X-ray beam to initiate electrons emission from the sample (Fig. 2.20). Since the mean free path of the emitted electrons

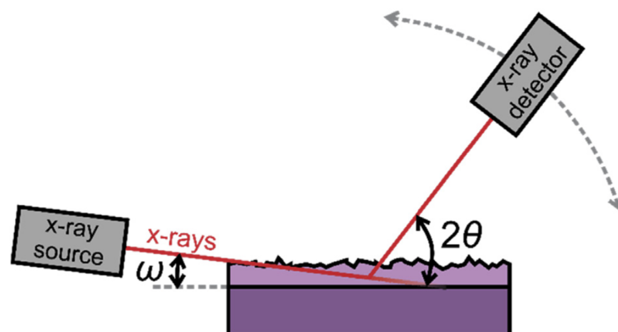

Figure 2.19: Schematic of measurement of thin film by grazing incidence angle XRD [27]

in solids is generally very short, only electrons from a surface selvage layer (less than $1nm$) contribute to the analysed signal. The electrons have characteristic energies corresponding to the emitting atom orbital levels. From analyzing the energetic spectrum of characteristic photoelectrons, it is possible to find out the elemental composition of the tested sample surface, as well as the types of chemical bonds. Thus, the XPS method suits for very precise chemical analysis of the sample surface [28] [29].

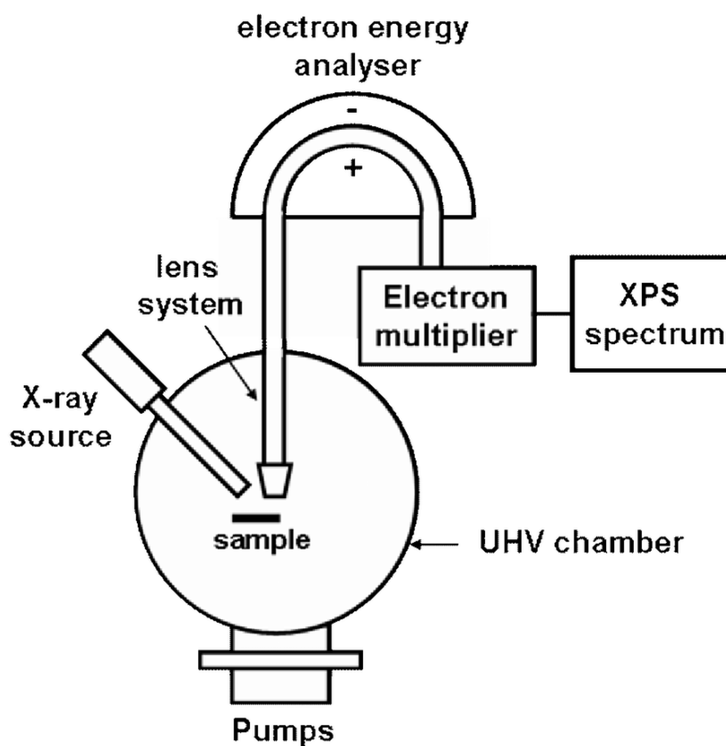

Figure 2.20: Schematic of XPS setup [29]

Confocal Microscopy

The confocal microscopy is an optical method for examination of surface morphology. The confocal microscopy uses a laser beam that travels trough a confocal aperture to the sample. Light scattered from only a very small spot which is in the center of the focus is examined at one moment (Fig. 2.21). This allows the microscope to scan the desired area of the sample and to create a precise 2D or 3D map of the sample surface. The confocal microscopy can also be used for thin film thickness measurement. To measure the thickness, it is necessary to have a sharp edge between the film and the free substrate surface prepared on the tested sample. The microscope scans over the substrate/film boundary (edge). The film thickness is then determined from the changes in focus position [30].

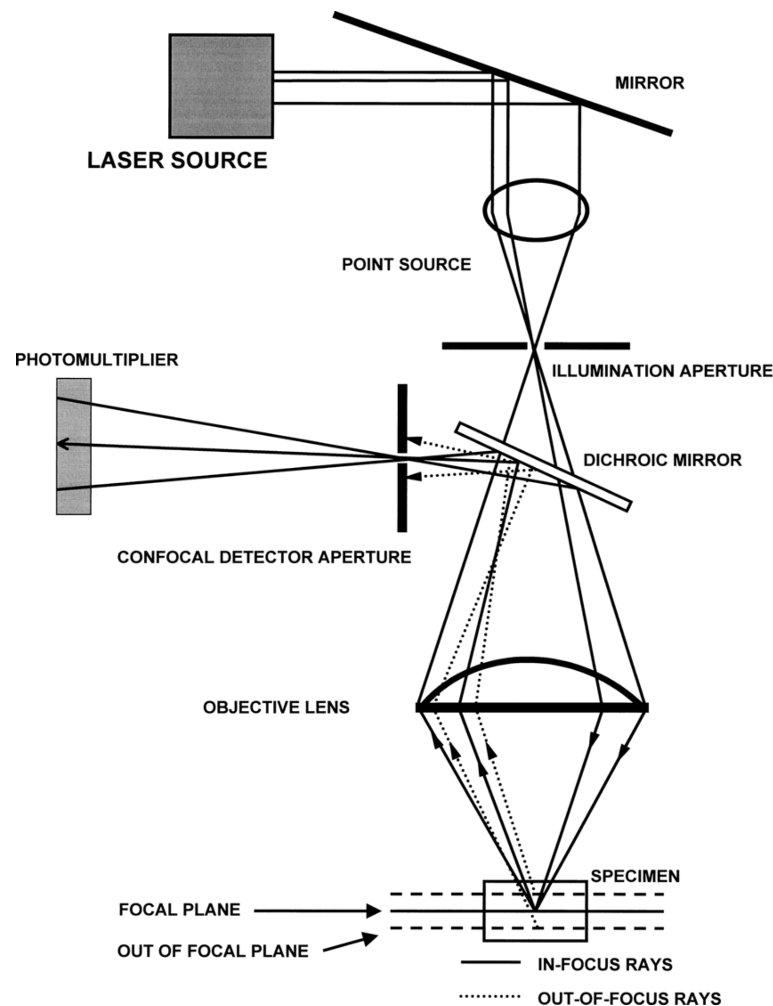

Figure 2.21: Schematic illustration of the confocal microscopy setup. [31]

2.4 High Temperature Superconductors

The effect of superconductivity was discovered by Kamerlingh Onnes in 1911. The transition from the normal to the superconducting state is bounded by critical temperature, below which superconductors show zero electrical resistance and ideal diamagnetic properties. Theoretically, the superconductivity was first described by so called Bardeen Cooper Schrieffer (BCS) theory in 1957. According to this theory, the superconductive state is possible to achieve only for the temperatures bellow 30 K. The HTS, which break this limit, are defined as the superconductors with the critical temperature exceeding 30 K. Sometimes, it is also the boiling temperature of liquid nitrogen (77 K) used as the critical temperature defining the group of HTS [32]. The practical importance of the liquid nitrogen is here in its relatively low fabrication cost and the relative ease of use.

The high temperature superconductors can be further subdivided according to their chemical composition and crystalline structure into families of magnesium diboride, iron based superconductors and cuprates [33]. This thesis is focused on the latter group, namely on the compounds characterized by the summary formula $Y_1Ba_2Cu_3O_{7-x}$ [34].

Superconductors can be also classified by their response to external magnetic field. Superconductors of the type I show a single critical field value above which the material loses all superconductive properties. Superconductors of the type II are characterized by two different critical magnetic field values between which the material exhibits existence of an intermediate phase, mixing together the ordinary and superconducting properties. The state is called "vortex" state, due to the existence of a vortex lattice within in the superconductor volume. Above the second critical field, the type II superconductors lose all superconducting properties.

2.4.1 YBCO Structure and Properties

The $Y_1Ba_2Cu_3O_{7-x}$ (frequently abbreviated as "YBCO") is one of the most common high temperature superconductor prepared and used today. It has a perovskite type of crystalline structure, with a $Cu-O$ sublattice consisting of two CuO_2 planes perpendicular to the c axis and $Cu-O$ chains along top the a axis direction (Fig.2.22).

The yttrium atoms separate the CuO_2 planes. It is assumed that the CuO_2 planes are the main source of the high temperature superconductivity effect, however, any definite proven theory of the high temperature superconductivity is still not available. The superconductive properties also strongly depend on the amount of oxygen present in the compound. Stoichiometry

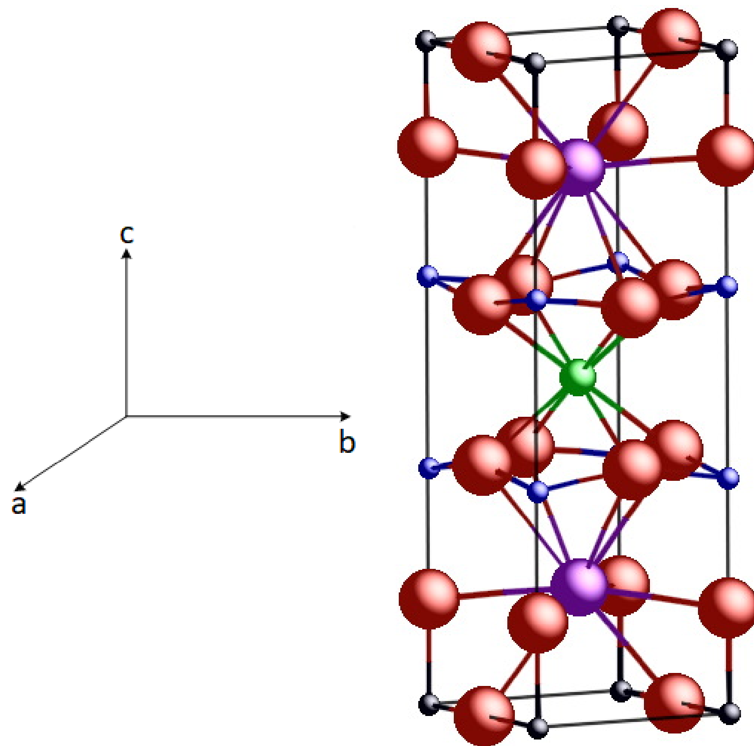

Figure 2.22: Elementary cell of YBCO crystalline structure, the oxygen, barium, copper and yttrium atoms are marked in red, purple, blue and green color, respectively [35]

$Y_1Ba_2Cu_3O_6$ lacks the necessary oxygen and does not exhibit superconductive properties. The minimal amount of oxygen necessary for the HTS effect to exist has been found as being equal to the stoichimetry $Y_1Ba_2Cu_3O_{6.4}$ (Fig.2.23) [36]. Best superconductive properties reported corresponds then to the stoichimetry $Y_1Ba_2Cu_3O_{6.93}$ [34]. With the oxygen content increasing, the YBCO crystalline structure also changes from a tetragonal structure with the space group $P4/mmm$ to the orthorombical structure with the space group $Pmmm$ [37].

For achieving the correct structure during a thin film deposition, it is necessary to heat up sufficiently the substrate. The temperature window within which the superconductive structure $Y_1Ba_2Cu_3O_{7-x}$ grows is between $760°C$ to $820°C$ [38] [39]. This temperature may change when using different deposition techniques and/or different substrate materials. Unfortunately, at this temperature, the material looses oxygen crucial for the superconductive properties, as mentioned above. Thus, the sample has to be annealed after deposition in order to obtain the right structure with the correct amount of oxygen. The annealing is usually done in the oxygen atmosphere at the temperatures around $400°C$ [40].

For preparation of YBCO thin films by IJD, the mostly used one is a sintered target composed of the $Y_1Ba_2Cu_3O_{7-x}$. The $Y_1Ba_2Cu_3O_{7-x}$ is commonly prepared from precursors CuO, $BaCO_3$

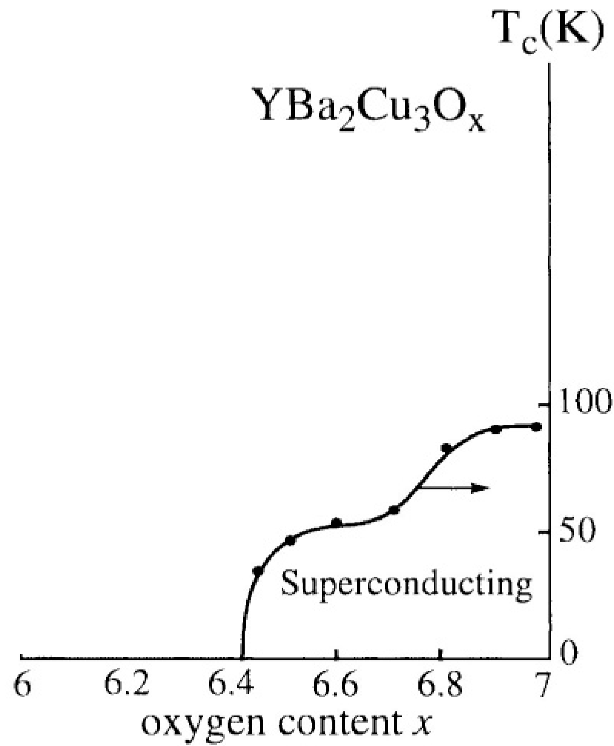

Figure 2.23: Influence of oxygen stoichimetry on the critical temperature of YBCO superconductors [36]

and Y_2O_3 see reaction below [41]. For the reaction to be valid, the condition $y = 0.5(1-2x)$ must be met. Through combination of these precursors, a number of other phases can arise, in addition to the desired phase $Y_1Ba_2Cu_3O_{7-x}$ (which is frequently abbreviated as $Y123$ Fig. 2.24).

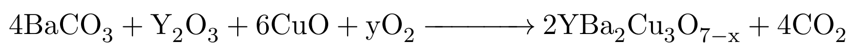

$$4BaCO_3 + Y_2O_3 + 6CuO + yO_2 \longrightarrow 2YBa_2Cu_3O_{7-x} + 4CO_2$$

The ternary phases $Y143$, $Y152$, $Y211$, as well as the other binary phases, does not exhibit superconductive properties. Only two superconductive phases of YBCO have been identified, the already mentioned $Y123$ and the $Y385$ [43]. During deposition of a thin film, if the deposition parameters are not correctly set, an undesirable decomposition into the basic precursors can take place, too [44].

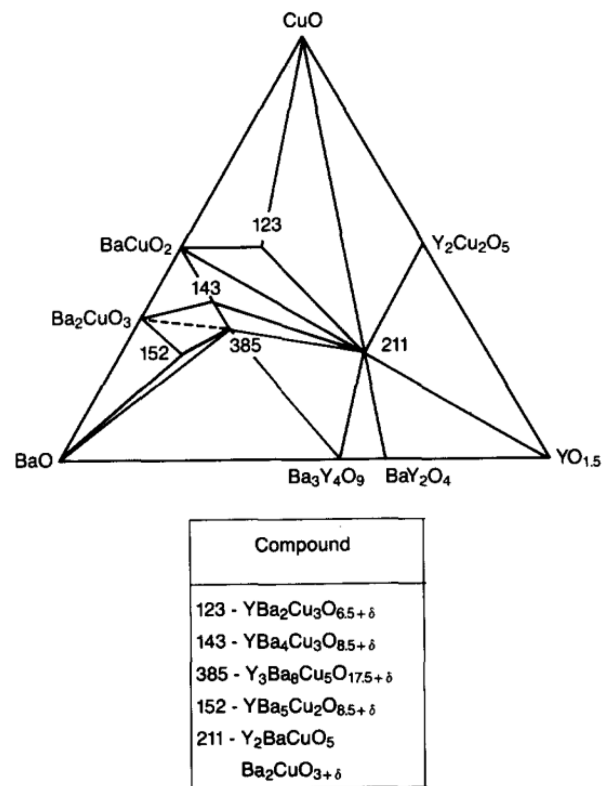

Compound
123 - $YBa_2Cu_3O_{6.5+\delta}$
143 - $YBa_4Cu_3O_{8.5+\delta}$
385 - $Y_3Ba_8Cu_5O_{17.5+\delta}$
152 - $YBa_5Cu_2O_{8.5+\delta}$
211 - Y_2BaCuO_5
$Ba_2CuO_{3+\delta}$

Figure 2.24: The ternary phase diagram of BaO-CuO-Y_2O_3 system [42]

3 Experimental

The main aim of this thesis is to analyse in depth the IJD deposition process and influence of its main parameters on properties of the resulting HTS films and, through this analysis, to collect knowledge necessary for successful fabrication of HTS films showing superconducting behaviour. The search process for the right deposition parameters is a relatively complex problem treated in this thesis by a semi-empirical approach. The deposition process has been separated onto several experimental parts/steps. Each set of experiments is designed to examine a different selected deposition parameter and its influence onto the prepared HTS films. The initial conditions for each step were chosen based on the available published information as well as on the general experience from previous thin film preparation using the IJD method.

Several parameters were fixed during the whole examination process, due to the small operation window of IJD for these parameters, following from previous studies; the working gas type, its composition and its pressure. Pure oxygen is selected as the working gas throughout the studies. Its working pressure is then fixed since the working conditions of IJD source has to be conformal with Paschen law.

3.1 Accelerating Voltage and Substrate Positioning

The distance between the substrate and the target is a relevant parameter with influence on the energy of particles approaching the substrate. The placement of substrate in a right position is thus very important for character of the thin film growth process. A detail description of the plasma travel process during the IJD deposition, affecting mainly the ideal distance between the substrate and the target has been already given in Section 2.1.3. For its key importance, the substrate positioning was already analysed in many studies dealing with deposition of thin films by IJD method [8], [28], [45] and [46]. The optimal distance following from that extensive data evaluation amounts 110mm.

The accelerating voltage value affects the energy of electron pulse coming to the target. According to the the equation 2.2, the energy of electrons influences their penetration depth i.e, it correlates with the amount of the ablated material. The latter then further affects the speed and quality of the resulting layer growth.

The testing set consisting of three samples was prepared in order to examine the influence of acceleration voltage on the surface morphology playing an important role in the application of HTS films in industry. From previous experience with IJD, three different values of accelerating voltages were chosen: 10 kV, 12 kV and 14 kV. Accelerating voltage values lower than 10 kV were avoided with regard to the resulting low growth rate leading to too long deposition times. Higher deposition energies, on the other hand, result in creation of large density of impurities in the form of "droplets" or "splashes", both highly undesirable [46]. For detailed overview of the deposition parameters used for the first sample set see Table 3.1.

Table 3.1: Deposition parameters for the set of samples used in examination of acceleration voltage influence

Name	ML,Y-123,900/12	ML,Y-123,900/12	ML,Y-123,900/12
Distance [mm]	110	110	110
Acceleration voltage [kV]	10	12	14
Deposition time [min]	15	15	15
Frequency [Hz]	10	10	10
Substrate	tape+Si wafer	tape+Si wafer	tape+Si wafer
Substrate temperature [$^\circ C$]	R.T.	R.T.	R.T.

Morphology of the prepared thin films was then analyzed by SEM (see Fig.3.1). After evaluation of morphology of the prepared samples, the acceleration voltage of 14 kV was identified as the best one from the options tested. This value was chosen and fixed during the next investigation steps focused on influence of the target mechanical properties on the

deposition process. Main reason for choosing the latter voltage consisted in the number of "droplets", appearing on the film surface and falling down with the acceleration voltage increasing. The second reasons is the growth rate, rising up with the acceleration voltage value growing. Achievement of high growth rate is important and desirable, since thicker films allow for reducing / avoiding the substrate influence during the subsequent morphology analysis.

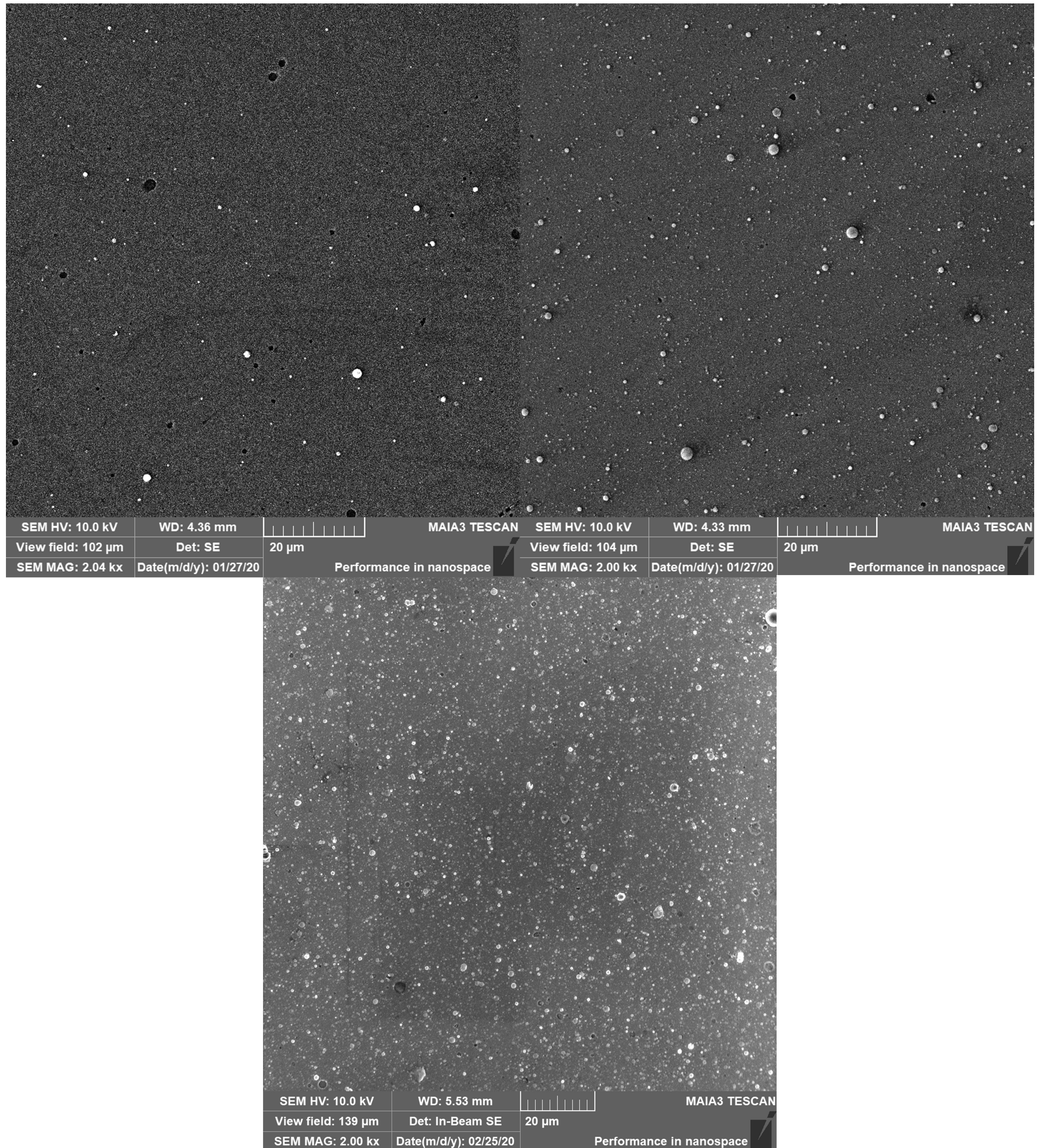

Figure 3.1: SEM images of the films prepared using acceleration voltage 10 kV (top left), 12 kV (top right) and 14kV (bottom); Tescan MAIA3 scanning electron microscope

3.2 Target Density

The properties of targets play a crucial role in the preparation of HTS thin films using IJD. This paragraph concentrates on the problem how the mass density of the used target affects the properties of the prepared thin films. From equation 2.2, it is possible to deduce the influence of the target mass density on the penetration depth of electrons. This penetration depth then closely correlates with the deposition yield per one IJD head pulse. The amount of material deposited during single pulse defines then the speed of growth and the morphology of the resulting surface.

The targets used to test the influence of mass density were prepared from the powder $Y_1Ba_2Cu_3O_{7-x}$, obtained by mixing precursors Y_2O_3, $BaCO_3$ and CuO in the stoichiometric ratio. Target powder was then calcined in four steps at temperatures from 850° to 880° with homogenization between the steps. Each of the targets was formed by uniaxially pressing $18g$ of the raw powder into a disk with diameter 32 mm. In order to obtain different final densities, the targets were sintered at different temperatures and for different lengths of time. From the set of 18 prepared targets, total of 9 with equal difference in mass density were chosen for subsequent experiments (see Fig.3.2). Let´s notice that the theoretical maximal density of the phase $Y123$ is $6.3g/cm^3$ [47]; this density is not easily achievable and thus not often used.

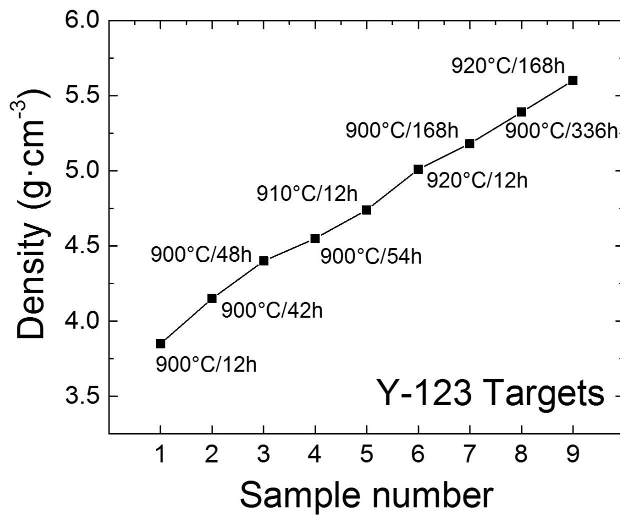

Figure 3.2: Mass densities of the prepared targets and the main preparation parameters (furnace temperature and the dwell time)

3.2.1 Thickness

The films prepared by IJD using the nine selected testing targets were deposited on two different substrates at once. The first substrate consisted of a monocrystalline Si wafer; a special metallic tape with buffer layers for YBCO deposition was then selected as the second substrate type. At first, the resulting layer thickness was examined by confocal microscopy method. As explained in the Section 2.3, the confocal microscope can be used to analyse thickness of film when a sharp step between the layer and the substrate exists / is prepared during the deposition (see Fig. 3.3). In the performed experiments, the confocal microscope (Sensofar S neox, Spain) with 5Mpx camera was used to measure the thickness and 3D surface of the prepared thin layers. A 150x objective with a working distance of 1.5 mm from the sample was used. The microscope was equipped with four LEDs: Red (630 nm); green (530 nm); blue (460 nm) and white (575 nm; center) and Ai Focus Variation designed for measuring of thin films. Senso MAP and SensoPRO software was used to process the recorded data.
For thickness measurement, a 2D profile is sufficient. Fig.3.4 shows an example of profile measured on the edge of a HTS layer. Presence of local profile peaks is apparent, the latter corresponding to the droplet-like surface irregularities on the surface of the prepared film. The thickness is obtained as the mean leverage of the right side of the profile that corresponds to the layer.
This procedure was applied for all prepared layers. The obtained film thickness values are summarized in Table 3.2.

As already mentioned, the equation 2.2 binds together the mass density of the target and the depth of electron penetration which directly affects the amount of ablated material. The influence of target density on the calculated penetration depth and measured layer thickness is demonstrated in Fig. 3.5. It is possible to see that both dependencies have similar trends. The largest deviations are found for both the minimal and maximal target density, which fact is probably due to the influence of other phenomena growing in their influence at these density margins.

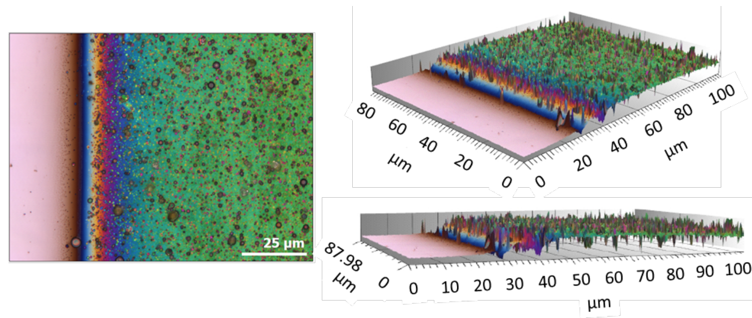

Figure 3.3: Example of 2D (left) and 3D (right) picture of prepared layer surface recorded by confocal microscope; target with mass density $5.4 g/cm^3$ used for deposition; edge of the layer is clearly visible

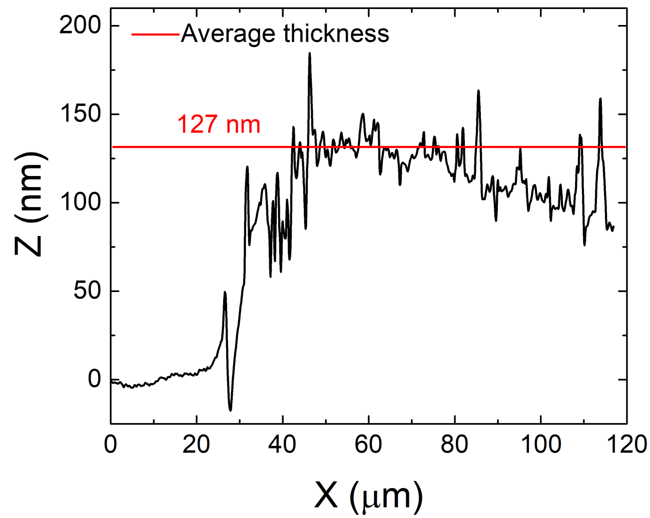

Figure 3.4: Example of thickness profile of the film grown with target of the mass density $5.4\ g/cm^3$

Table 3.2: The film thickness grown from the targets with indicated mass densities; identical IJD growth conditions were applied for all the prepared films

Target density$[g/cm^3]$	Film thickness$[nm]$
3.85	205
4.15	162
4.4	150
4.55	157
4.74	146
5.01	123
5.18	126
5.39	127
5.6	104

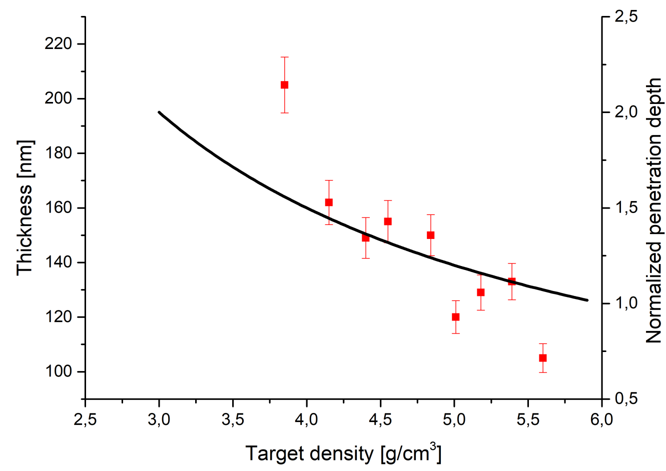

Figure 3.5: Normalized penetration depth depending on the density of the target (full line) combined with the experimentally obtained thickness of the grown films (full squares with ESD indicated)

3.2.2 Surface Morphology

Amount of material transported during one deposition pulse not only contributes to the variations in the final thickness, but also plays an important role in the surface morphology of the resulting films. The surface morphology is then a key parameter for deposition of cover layers onto the HTS layer, as already been described in the Subsection 2.4.1. The common phenomena observed in preparation of thin films by IJD is the presence of "droplets" appearing on surface of the prepared films [46]. As shown in Fig. 2.15 on the example of Al_2O_3 layer, the "droplets" are distinguishable on the surface topology profiles, but the underlying volume of film is homogeneous without any visible impurities, boundaries, pores, etc.

Quantitative analysis of the surface topology was done by a software for image processing. Several softwares packages were tested, namely Gwyddion, Matlab and ImageJ. The best results of the SEM image analysis were achieved with the software ImageJ. The main goal of the examination was to find out a relation (if any) between the frequency of the "droplets" presence and the used target densities. In particular, the size, amount and total area covered by the "droplets" were examined.

The analysis process by Imagej consisted in several steps. First, it was necessary to select the examined area of the SEM image. Then the particles in the selected area had to be visualized on the basis of correctly set contrast threshold. The identified particles were then approximated by elliptical boundaries used afterwards to determine the total count and total area of "droplets" (see Fig.3.6).

The SEM micrographs for all tested target densities are collected in the Fig. 3.7. The average size, amount and total area covered by "droplets" are given in the Table 3.3. From the obtained data, it is not easily noticeable any simple functional dependence between the "droplets" properties and the target densities. The minimum surface coverage is found for the "intermediate" target mass densities 4.55 and 4.84 g/cm^3, showing also the smallest mean size of the droplets.

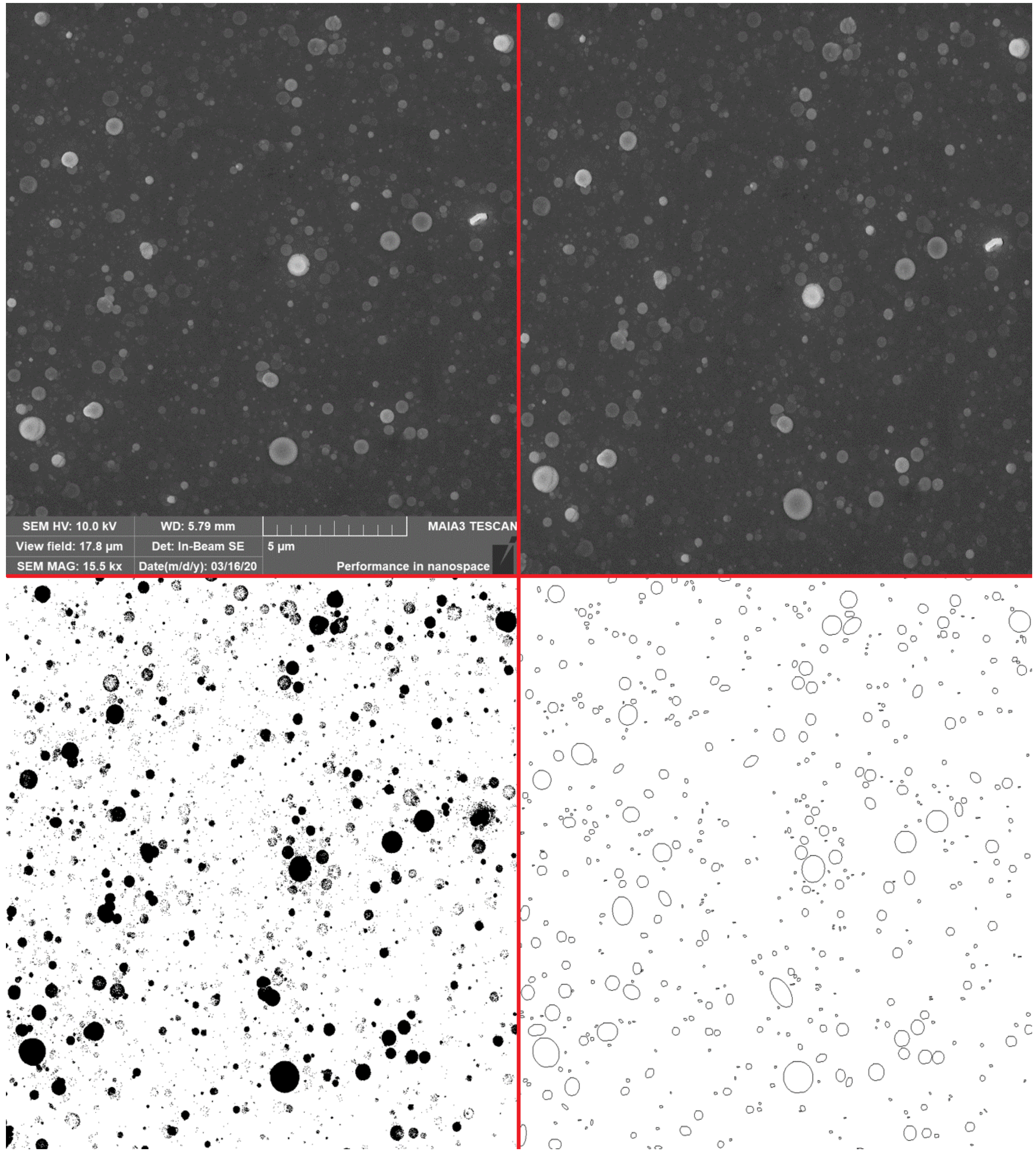

Figure 3.6: Example of the image processing steps applied in the surface topology analysis of the prepared layers performed by ImageJ software; the used target density 4.84 g/cm^3. Original SEM micrograph (top left), selected area for examination (top right), B/W converted picture with contrast threshold set (bottom left), isolated particle boundaries (bottom right)

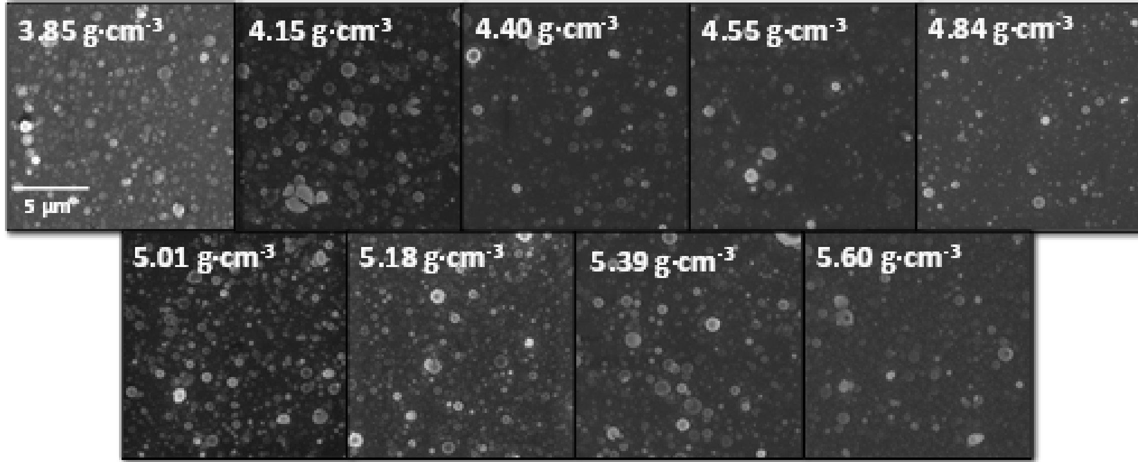

Figure 3.7: Original SEM snaps of layers prepared from targets of different density.

Table 3.3: The characteristics of surface droplets obtained from topological analysis of SEM micro-graphs shown in Figure 3.7

Target density	Average particle size [μm]	Number of particles	Coverage [%]
3.85	1.30	383	3.85
4.15	2.81	353	7.66
4.40	1.70	320	4.21
4.55	0.93	350	2.52
4.84	0.68	563	2.14
5.01	2.37	470	7.01
5.18	1.02	785	3.03
5.39	2.68	305	6.33
5.60	1.54	274	3.26

3.3 Chemical Composition of Target

The stoichimetry of YBCO superconductors plays a crucial role in their superconductive behavior. The chemical system has several stable phases, which were introduced in the Subsection 2.4.1. Some of these phases are very similar in their composition, but differ in their properties. Supposing there is a close relationship between the composition of the deposition target and the stoichiometry of the grown layer, it is necessary to fine-tune the chemical stoichimetry of the deposition target very carefully in order to achieve the resulting thin films containing the correct superconducting phase [48]. With the target chemical composition fixed, the exact composition of the growth film is determined by the IJD transport coefficients determining the elemental transport from the target to the film.

To investigate the transport coefficient for IJD deposition, seven targets with different stoichimetry were prepared. The desired stoichiometric ratio of the targets was obtained by variation in mixing the precursors Y_2O_3, $BaCo_3$ and CuO. The obtained target samples are marked according to their stoichiometry (oxygen content is omitted). Preparation of the target powders consisted in a four-step calcination, with homogenization applied between each of these steps. The calcination steps were performed at temperatures ranging between $850°C$ and $880°C$. The resulting powder was then uniaxially pressed into the disks with diameter 32 mm and weight of 50 g. The following targets were prepared: $Y_1Ba_{1.5}Cu_3O_x$, $Y_1Ba_2Cu_3O_x$, $Y_1Ba_{2.5}Cu_3O_x$, $Y_1Ba_{2.5}Cu_{3.5}O_x$, $Y_1Ba_2Cu_{3.5}O_x$, $Y_1Ba_2Cu_4O_x$, and $Y_1Ba_2Cu_{4.5}O_x$.

3.3.1 Transport Coefficients

The transport coefficient of selected element is defined as the ratio between the atomic content of the element in the target and the content in the prepared thin film. All other parameters of deposition were fixed: distance 110 mm, acceleration voltage 14 kV, deposition time 30 min, frequency of pulses 10 Hz and substrate temperature $650°C$. Si wafer was used as substrate, since it does not interfere with the composition of the prepared thin films.

The examination of chemical composition was performed by an EDS analyzer (X-Max 150) with a 20 mm^2 silicon drift detector (SDD, Oxford Instruments). This analyzer is part of the scanning electron microscope (SEM) Tescan MAIA3. The data were analyzed by using the AZtecEnergy software. Prior measurement, all samples were placed onto conductive carbon tape. The measurements were performed in the high-resolution mode with the acceleration voltage 10 kV. This spectroscopic method is closely described in the Subsection 2.3.

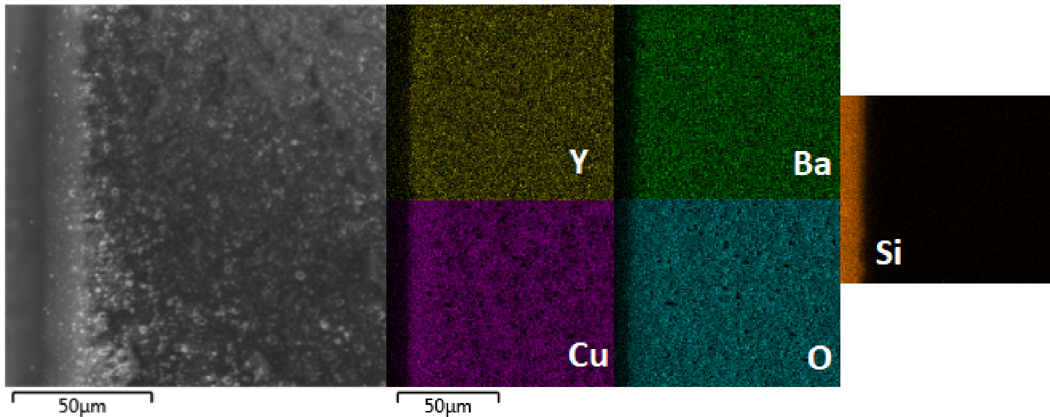

Figure 3.8: Example of the obtained distribution of the marked elements in the prepared thin film and in the substrate. The film was prepared from the $Y_1Ba_2Cu_3O_x$ target; the SEM view of the surface is shown on the left-most picture

Distribution of the elements over the tested film area was found as homogeneous. This conclusion follows from the obtained EDS maps (see Fig.3.8). Since the measurements were done in proximity of the sharp edge of the film (see Fig.3.9), the signal from Si substrate is also visible.

Figure 3.9: Picture of the thin film with the arrow pointing to the edge where the EDS was measured

Data from the EDS measurements have form of atomic stoichiometry percentage of elements (see Fig.3.10). The observed presence of carbon is a known consequence of the measuring system contamination [49]. The signal from silicon follows from the fact that the HTS layer thickness is lower than the penetration depth of the exciting primary electron beam, allowing thus for collection of the signal coming from the substrate. The oxygen is not taken into account in the calculations of the transport coefficients, since it can be easily released from the structure of the film during deposition and its transport coefficient is therefore poorly defined for the deposition of a YBCO type superconductor.

After deposition, all samples have to be additionally oxygenated in order to achieve superconducting properties (as explained in the Subsection 2.4.1).

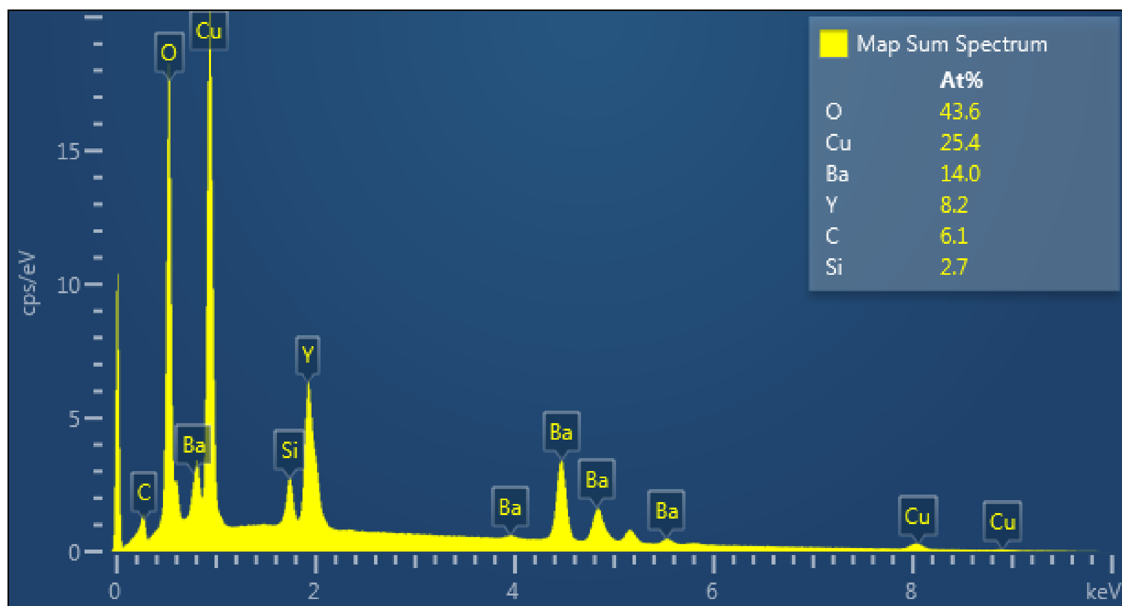

Figure 3.10: Example of the data obtained from the EDS analysis for the sample prepared from the $Y_1Ba_2Cu_3O_x$ target

The complete set of EDS composition data for each stoichiometry combination is shown in Fig. 3.11. Three sets of EDS measurements were performed: on the target before the first deposition, on the targets after the last deposition, and on the prepared thin films.

From the measured data, the transport coefficients were then calculated for each of the evaluated elements. The results are summarized in Tables 3.4 and 3.5.

Table 3.4: Transport coefficients for Y, Ba and Cu related to the targets´ composition before deposition

Targets	Y	Ba	Cu
$Y_1Ba_{1.5}Cu_3$	0.78	1.23	0.97
$Y_1Ba_2Cu_3$	0.83	1.10	0.97
$Y_1Ba_{2.5}Cu_3$	0.82	1.10	0.97
$Y_1Ba_{2.5}Cu_{3.5}$	0.48	1.15	1.09
$Y_1Ba_2Cu_{3.5}$	0.53	1.23	1.03
$Y_1Ba_2Cu_4$	0.91	1.22	0.89
$Y_1Ba_2Cu_{4.5}$	0.80	1.38	0.87

The correspondence in the chemical composition between the targets after deposition and the thin films is much better than those of the thin films and the targets before the deposition. The average difference in elemental composition between the targets after deposition and the corresponding prepared layers is less than 5%. This phenomenon is probably caused by a change in the chemical composition of the target at the beginning of deposition. The target is locally

Table 3.5: Transport coefficients for Y, Ba and Cu related to the targets´ composition after deposition.

Targets	Y	Ba	Cu
$Y_1Ba_{1.5}Cu_3$	0.89	1.05	1.03
$Y_1Ba_2Cu_3$	1.21	1.01	0.92
$Y_1Ba_{2.5}Cu_3$	1.01	1.01	0.97
$Y_1Ba_{2.5}Cu_{3.5}$	0.85	0.97	1.10
$Y_1Ba_2Cu_{3.5}$	0.86	0.97	1.08
$Y_1Ba_2Cu_4$	1.01	1.00	0.99
$Y_1Ba_2Cu_{4.5}$	0.90	1.05	1.01

extremely heated, which may lead to partial evaporation of some elements. Shutter in front of the samples was used for all other future preparations to prevent film growth before the target is stabilized.

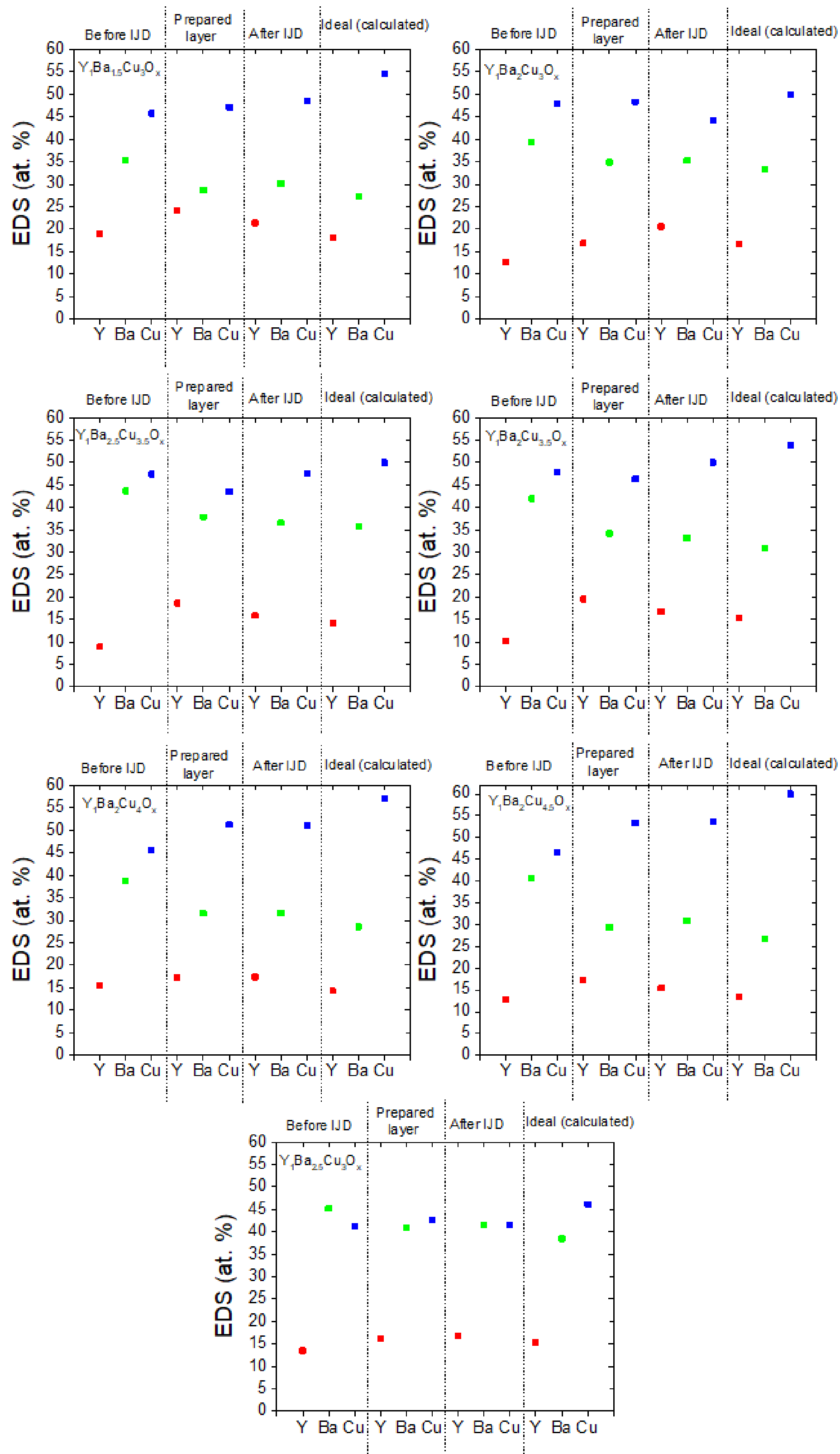

Figure 3.11: The atomic percentage of Y,Ba and Cu obtained from the EDS data for each initial stoichiometric composition and indicated type of measurement (on the fresh target, on the prepared layer, and on the target after IJD deposition).

3.4 Characterization of Structural Properties of HTS Films

The crystalline structure of the prepared thin films was analyzed by the X-ray diffraction (XRD) method. The XRD is a very powerful method for analyzing the real structure of polycrystalline materials, such as presence of structural phases, internal stresses and crystallographic textures. This method is described in more details in the Section 2.3.

YBCO materials form a relatively complex system with a number of different structural phases (see Fig.2.24). The growth of layer mass organized in a given crystallographic phase is affected by the exact chemical composition of the growing mixture, the type of substrate, and the temperature of the substrate. With the right choice of substrate, the epitaxial growth can be achieved, which is crucial for the growing layer orientation. As described in Section 2.4.1, REBCO-based high-temperature superconductors exhibit anisotropic superconducting properties, requiring to achieve a parallel orientation of the superconducting a-b planes with the substrate surface. The ideal thin film structure will have an extreme crystallographic texture with only (00l) reflections observable in a symmetric reflection position, and will consists purely of the $Y_1Ba_2Cu_3O_{7-\delta}$ phase.

A monocrystalline bulk sample supplied by Can Superconductors s.r.o. was measured at first and used as a reference standard. The monocrystalline bulk crystalline structure is oriented in the same way as it is necessary to orient the layers, and consists mainly of the $Y_1Ba_2Cu_3O_{7-\delta}$ phase with small amount of additional phases (see Fig.3.12). The most intensive observed diffraction lines correspond to the (00l) zone of the $Y_1Ba_2Cu_3O_{7-\delta}$ phase.

All measurement of the thin films samples were done with X´Pert PRO MPD (PANalytical) difractometer equipped with the X´Cellerator detector. The X-Ray source CoKα (α=0.179026 nm), was used, set into the grazing angle geometry. The angle between the primary beam and the film plane was 3°.

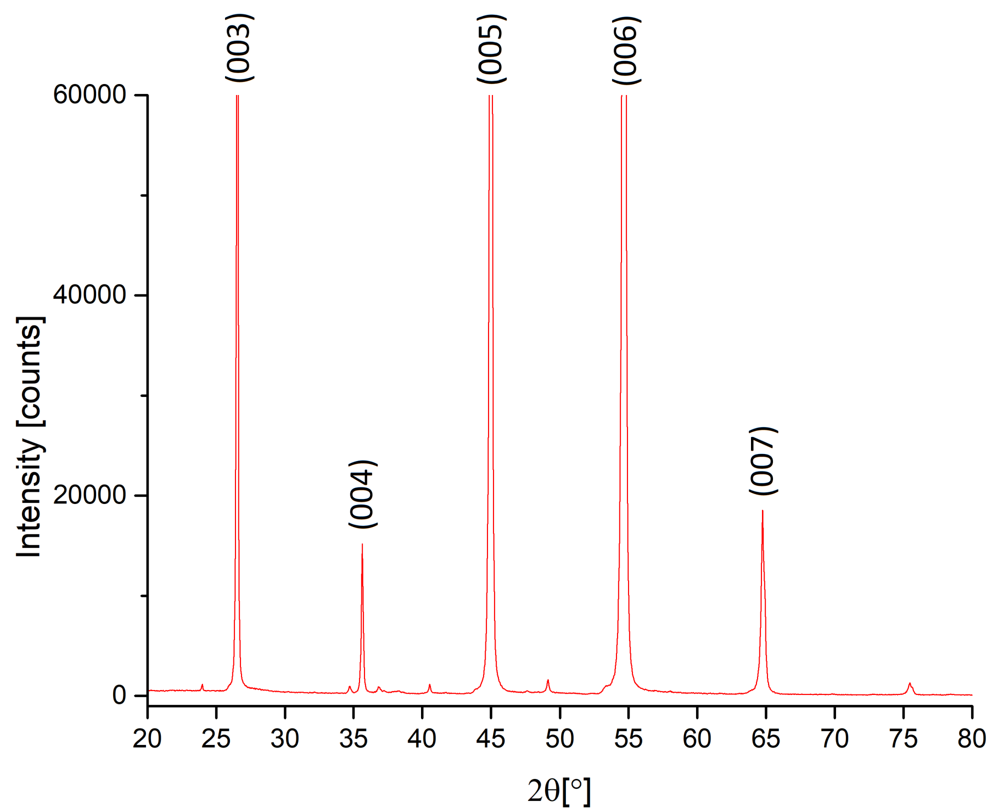

Figure 3.12: The XRD pattern of monocrystalline YBCO bulk, used as the standard, measured in Bragg-Brentano geometry; the bulk surface normal parallel to the scattering vector.

3.4.1 Influence of Substrate Type

Four different substrates were tested: monocrystalline Si(111), monocrystalline $LaAlO_3$(100), and two different special tapes for HTS deposition provided by companies Bruker (further on referrer as BruTape) and SuperOx (further on referrer as OxTape). To ensure the smallest possible layer difference caused by different conditions during deposition, all samples were prepared at once, within the single deposition run. The substrates were fixed on the special holder (see Fig.3.13) and, at least a part of each sample was within the main deposition cone where the growth of the film is most homogeneous. In the subsequent analysis, only the parts of samples with homogeneous thickness were used. The most obvious demonstration of thickness variations consists in the interference-caused colour changes of the reflected light visible eg. on the sample prepared on OxTape substrate (Fig. 3.13).

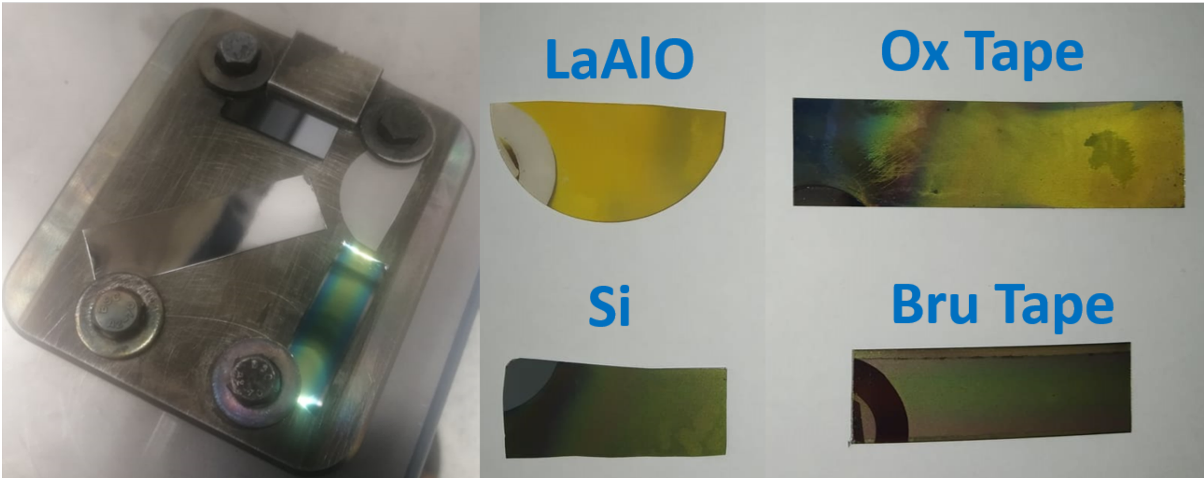

Figure 3.13: Substrates in the sample holder before deposition (left), and after deposition (right)

Table 3.6: Deposition parameters for the set of samples used in examination of the substrate influence

Sample name	Si	LaAlO	BruTape	OxTape
Distance $[mm]$	110	110	110	110
Acceleration voltage $[kV]$	14	14	14	14
Deposition time $[min]$	30	30	30	30
Frequency $[Hz]$	10	10	10	10
Substrate	Si (111)	$LaAlO_3$ (100)	Bruker tape	SuperOx tape
Substrate temperature $[°C]$	770	770	770	770

From the recorded XRD patterns (see Fig.3.14 and 3.15), it is clear that the growth of layers is really strongly influenced by the substrate type. On the two monocrystalline substrates tested, the films are decomposed into the precursor compounds, the effect being most likely caused

by the insufficient substrate temperature during deposition. On the BruTape and OxTape, it is possible to observe diffraction lines belonging to $Y_2Ba_1Cu_1$ phase, which might appear as transition phase before formation of $Y_1Ba_2Cu_3$ phase (see Fig.2.24). The unidentified diffraction lines on the tape samples might correspond to the diffraction from the buffer layers, or from the substrate itself. The tapes are made from a nickle alloy with a buffer layer of MgO and CeO. For each substrate, it is necessary to optimize the deposition parameters individually in order to obtain the desired superconductive phase.

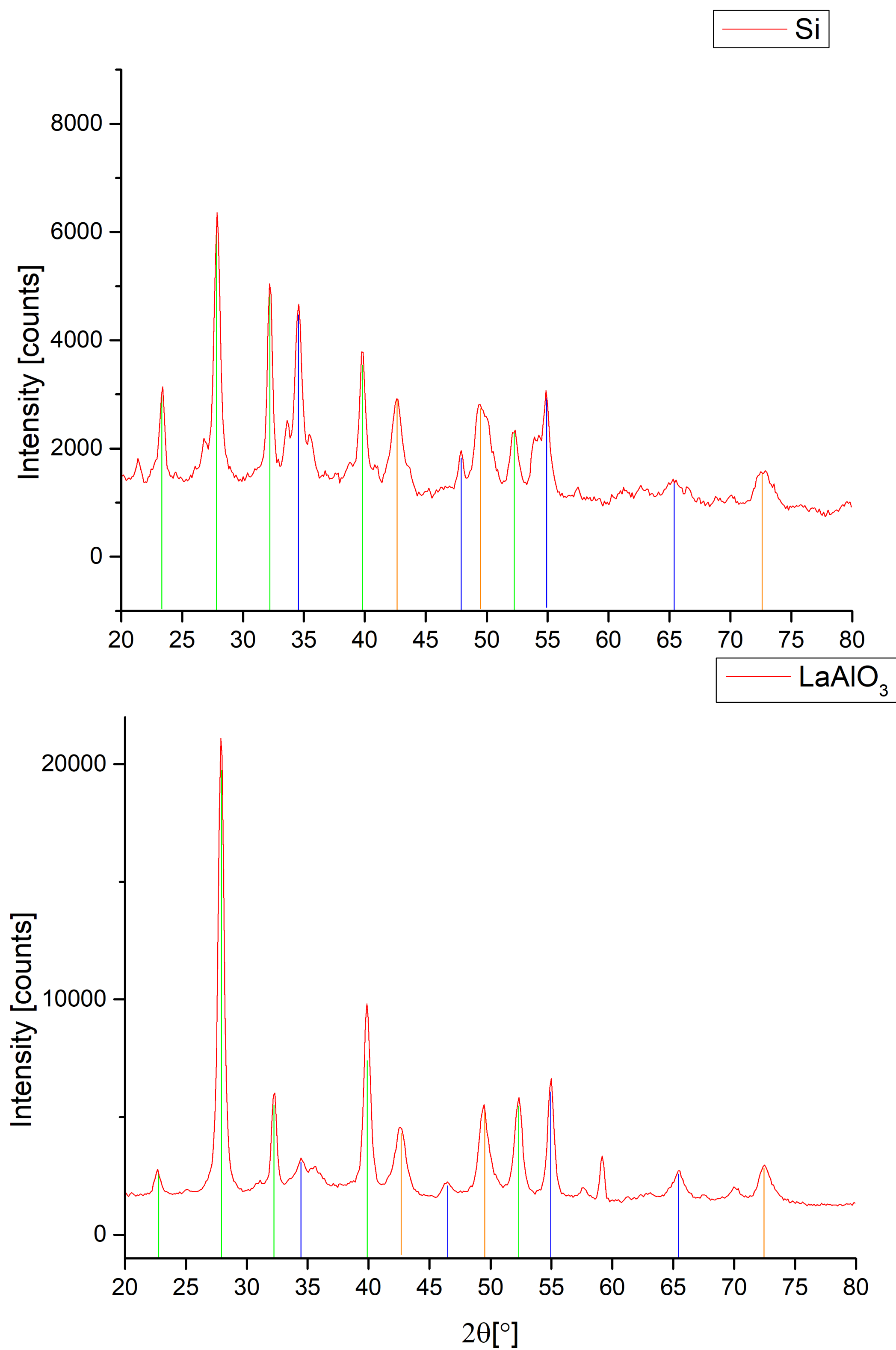

Figure 3.14: The XRD pattern of YBCO thin film on Si (111) and $LaAlO_3$ (100) wafer. GREEN marked diffraction lines corresponds to $BaCO_3$. ORANGE marked diffraction lines corresponds to Cu_2O. BLUE marked diffraction lines corresponds to Y_2O_3.

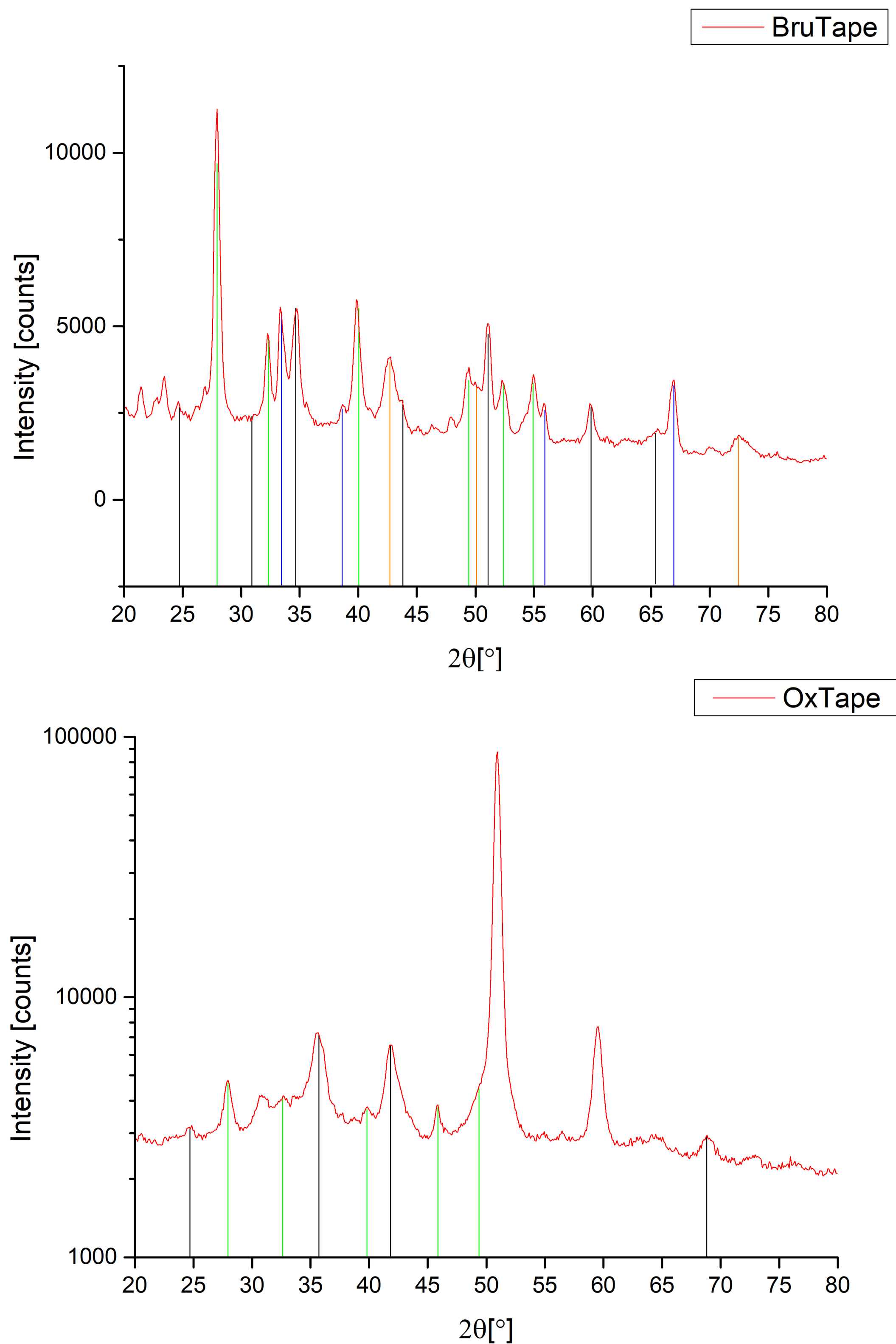

Figure 3.15: The XRD pattern of YBCO thin film on BruTape and on OxTape. GREEN marked diffraction lines corresponds to $BaCO_3$. ORANGE marked diffraction lines corresponds to Cu_2O. BLUE marked diffraction lines corresponds to Y_2O_3. BLACK marked diffraction lines corresponds to $Y_2Ba_1Cu_1$. Unmarked diffraction lines belong to the substrate

3.4.2 Influence of Substrate Temperature During Deposition

Setting the correct substrate temperature is crucial for successful deposition since it significantly affects the growth of $Y_1Ba_2Cu_3$ phase. According to [50], the right temperature window for preparation of desired $Y_1Ba_2Cu_3$ phase is around 780°C. However, the correct substrate temperature in various deposition system may vary due to the specifics of individual heaters and deposition techniques. Therefore, a careful examination of the relation between the substrate temperature and the phase composition has to be carried out specifically for each particular deposition system.

The BruTape substrate was chosen to test influence of the substrate temperature.The studied temperature window was between 700°C and 830°C, with addition of room temperature as a reference. The rest of deposition parameters for all samples was set to the values shown in Table 3.7.

Table 3.7: Deposition parameters for the set of samples used for examination of the substrate temperature influence

Sample name	YBCO(R.T.-830)
Distance [mm]	120
Acceleration voltage [kV]	14
Deposition time [min]	20
Frequency [Hz]	20
Substrate	BruTape
Substrate temperature [°C]	R.T.-830

Phase composition of the films prepared at the room temperature, and at 700°C is very similar. These films have broken down into $BaCO_3$(ICSD 00-005-0378), Cu_2O (ICSD 01-075-1531) and Y_2O_3 (ICSD 01-074-1828). In the XRD patterns of the sample deposited at 730°C, it is possible to observe an onset of phase transition from the individual precursors to the ternary system described in the Section 2.4.1. The most promising temperature range for sample preparation appears to be between 750°C and 770°C. Where phases $Y_2Ba_1Cu_1$ (ICSD 01-079-0238) and $CuYO_2$ (ICSD 01-077-2497) were identified. The samples prepared at these temperatures are very similar in their phase composition, corresponding to the ternary diagram shown in Fig. 2.24. At these temperatures, there is a chance that the desired phase $Y_1Ba_2Cu_3$ could be created if the composition were adjusted according to the data obtained in Section 3.3. The data obtained from EDS indicate that the prepared layers have a higher content of yttrium and a lower content of barium than the desired ratio necessary for the growth of the superconducting $Y_1Ba_2Cu_3$ phase. The last sample then, prepared at 830°C, is again partly broken down to the individual precursors,

but also contains $Y_2Ba_1Cu_1$. This result is probably caused by a too high temperature leading to decomposition of the ternary phases.

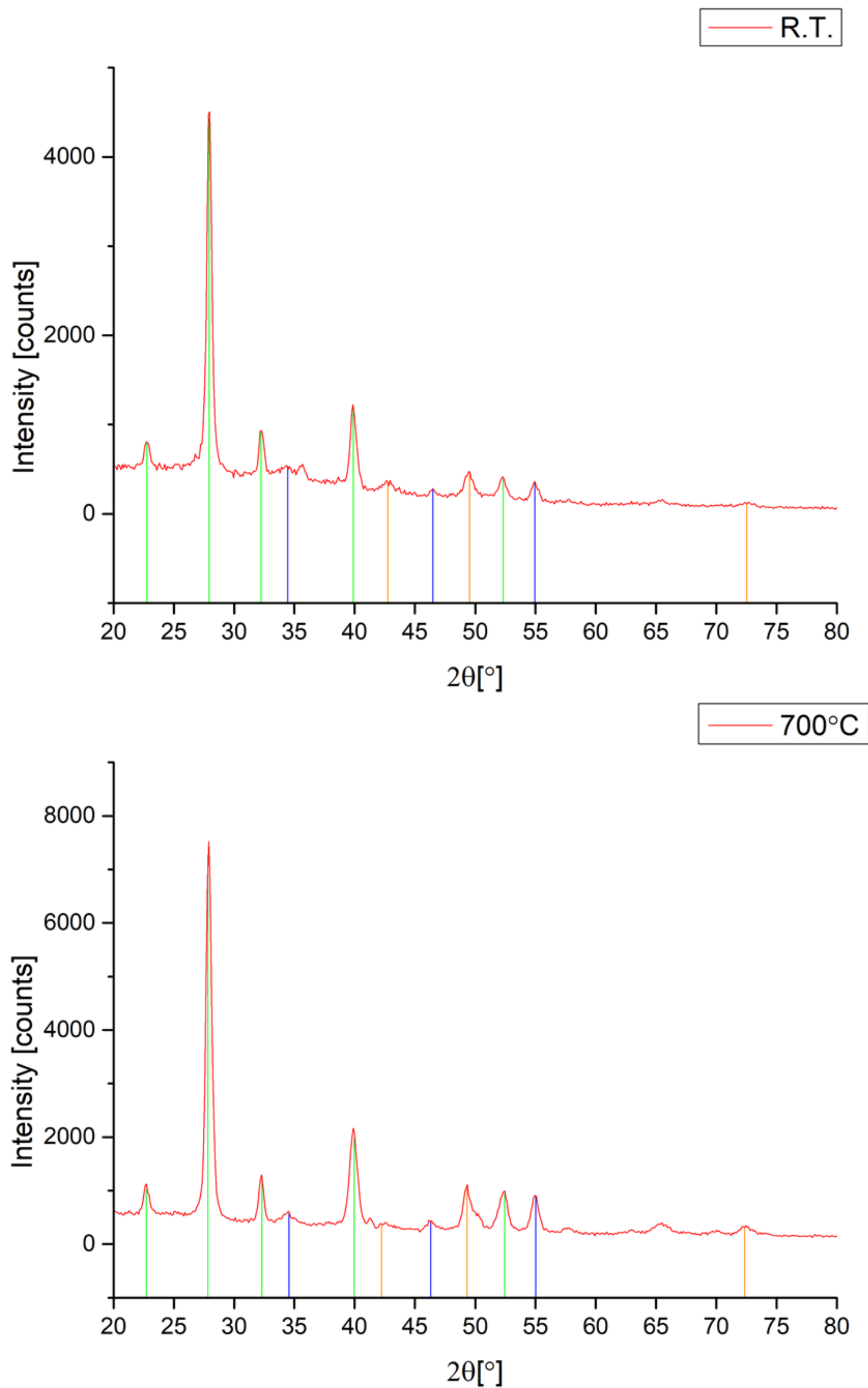

Figure 3.16: The XRD pattern of YBCO thin film deposited at the substrate temperature RT and 700°C GREEN marked diffraction lines corresponds to $BaCO_3$. ORANGE marked diffraction lines corresponds to Cu_2O. BLUE marked diffraction lines corresponds to Y_2O_3. BLACK marked diffraction lines corresponds to $Y_2Ba_1Cu_1$. RED marked diffraction lines corresponds to $CuYO_2$

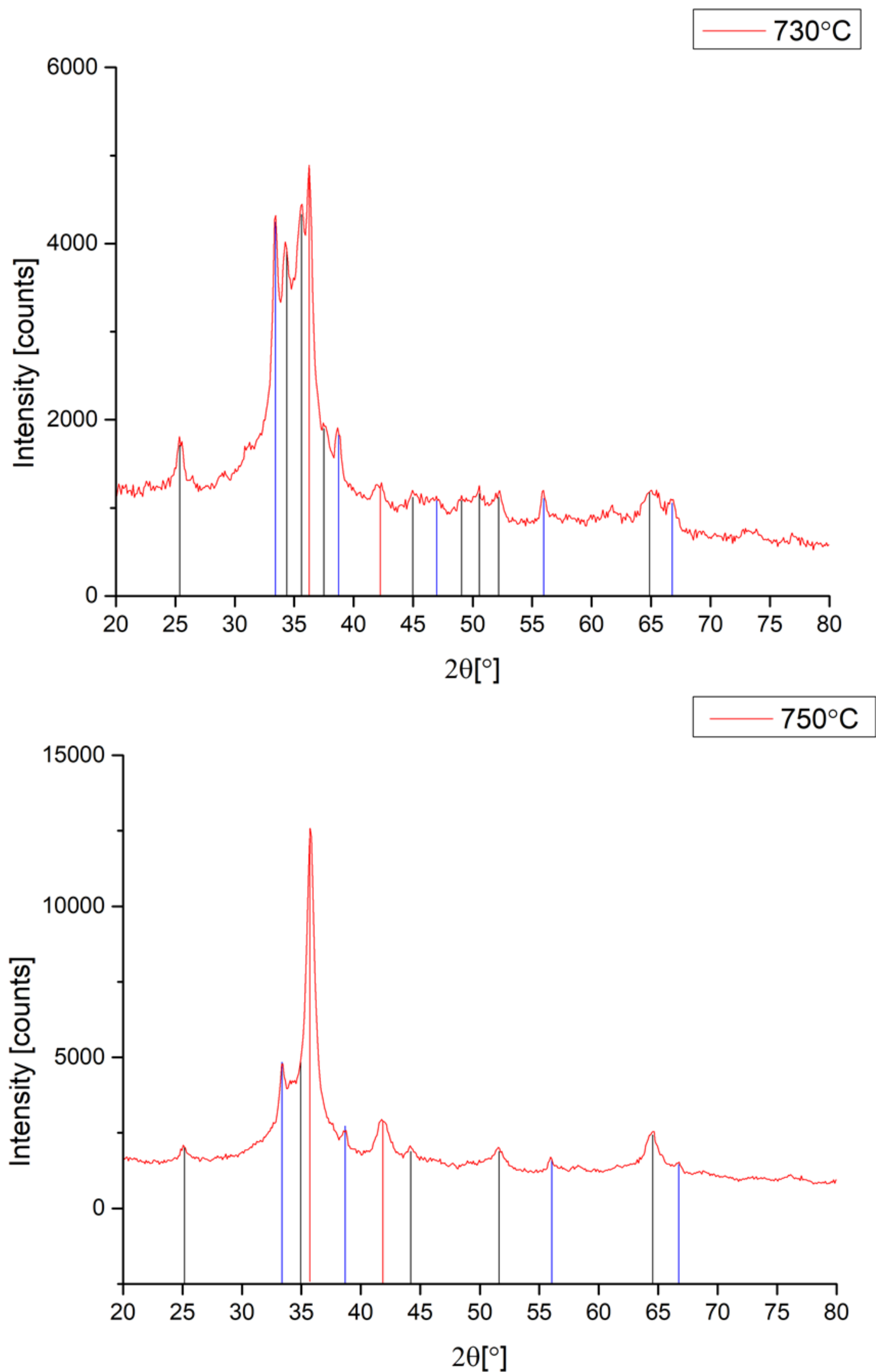

Figure 3.17: The XRD pattern of YBCO thin film deposited at the substrate temperature 730°C and 750°C GREEN marked diffraction lines corresponds to $BaCO_3$. ORANGE marked diffraction lines corresponds to Cu_2O. BLUE marked diffraction lines corresponds to Y_2O_3. BLACK marked diffraction lines corresponds to $Y_2Ba_1Cu_1$. RED marked diffraction lines corresponds to $CuYO_2$

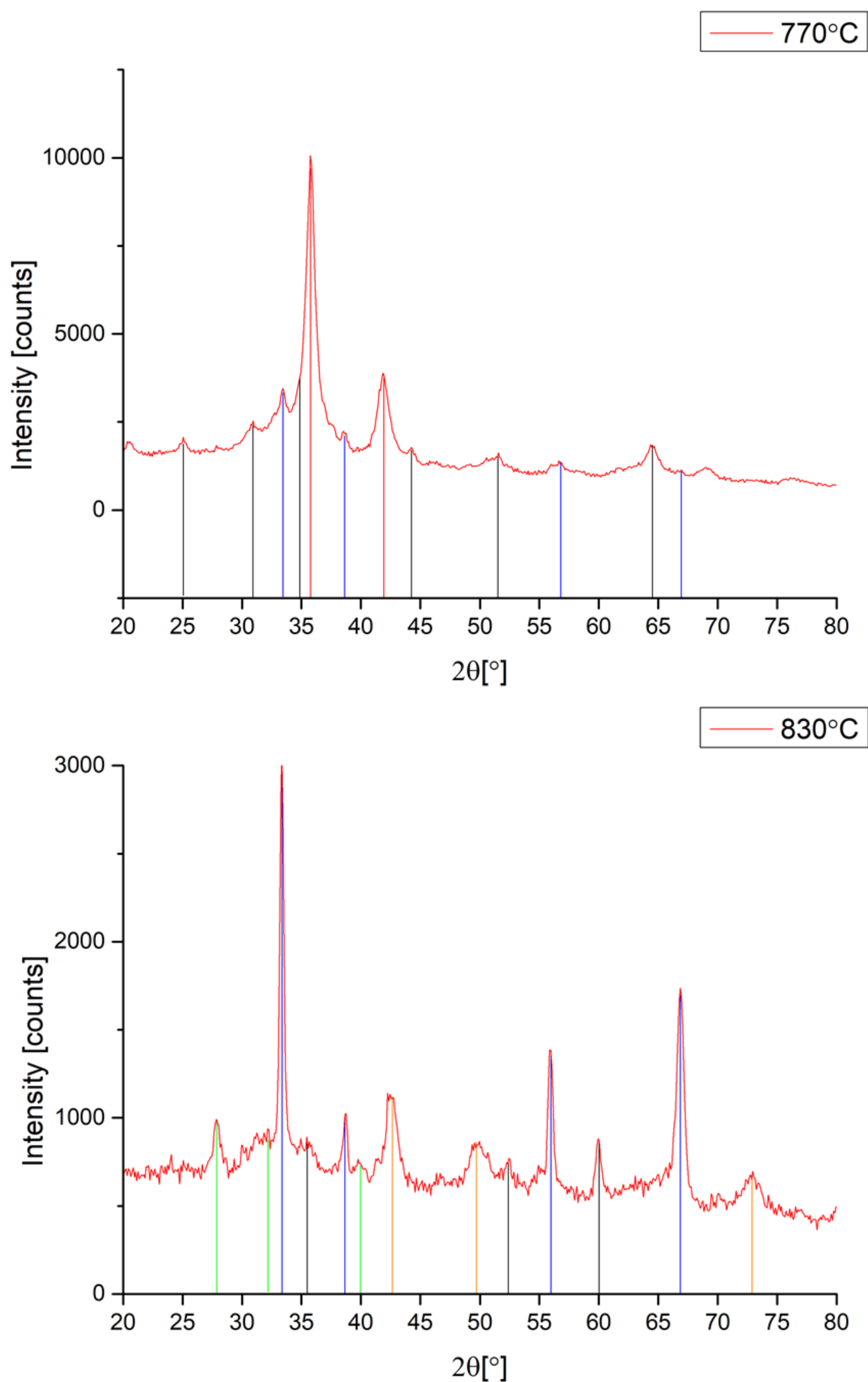

Figure 3.18: The XRD pattern of YBCO thin film deposited at the substrate temperature 770°C and 830°C GREEN marked diffraction lines corresponds to $BaCO_3$. ORANGE marked diffraction lines corresponds to Cu_2O. BLUE marked diffraction lines corresponds to Y_2O_3. BLACK marked diffraction lines corresponds to $Y_2Ba_1Cu_1$. RED marked diffraction lines corresponds to $CuYO_2$

3.4.3 Oxidation of Films

The amount of oxygen in REBCO materials plays a crucial role for superconducting properties as is closely described in Section 2.4.1. In the previous Section 3.4.2, it was shown that in order to obtain the desired phase, it is necessary to heat up the substrate to a temperature over $700°C$ at which, unfortunately, oxygen is released from the layer. Therefore, the samples have to be additionally oxidized after deposition. The oxidation tests were done in a furnace filled with the ambient atmosphere and kept at temperature of $400°C$ for 12 hours. For the oxidation tests, only the samples that underwent phase transformation were chosen i.e. the samples deposited with the substrate temperature exceeding $730°C$.

During the oxidation, most of the films mass decomposed into individual precursors. After oxidation, all tested films also contained a hard-to-identify phase. This might be the phase $Y_2Ba_1Cu_1$ which is very thermally stable and therefore should not decompose. However the diffraction lines that could correspond to this phase (marked black in the figures), especially the one at 60 degrees, do not correspond exactly to the theoretical position expected for this phase. The discrepancy can be caused e.g. by presence of internal stresses in the layer, incorporation of impurities or oxygen into the crystalline lattice of this phase or influence of crystallographic texture. The mentioned phenomena can change the position of the diffraction lines and/or their intensity.

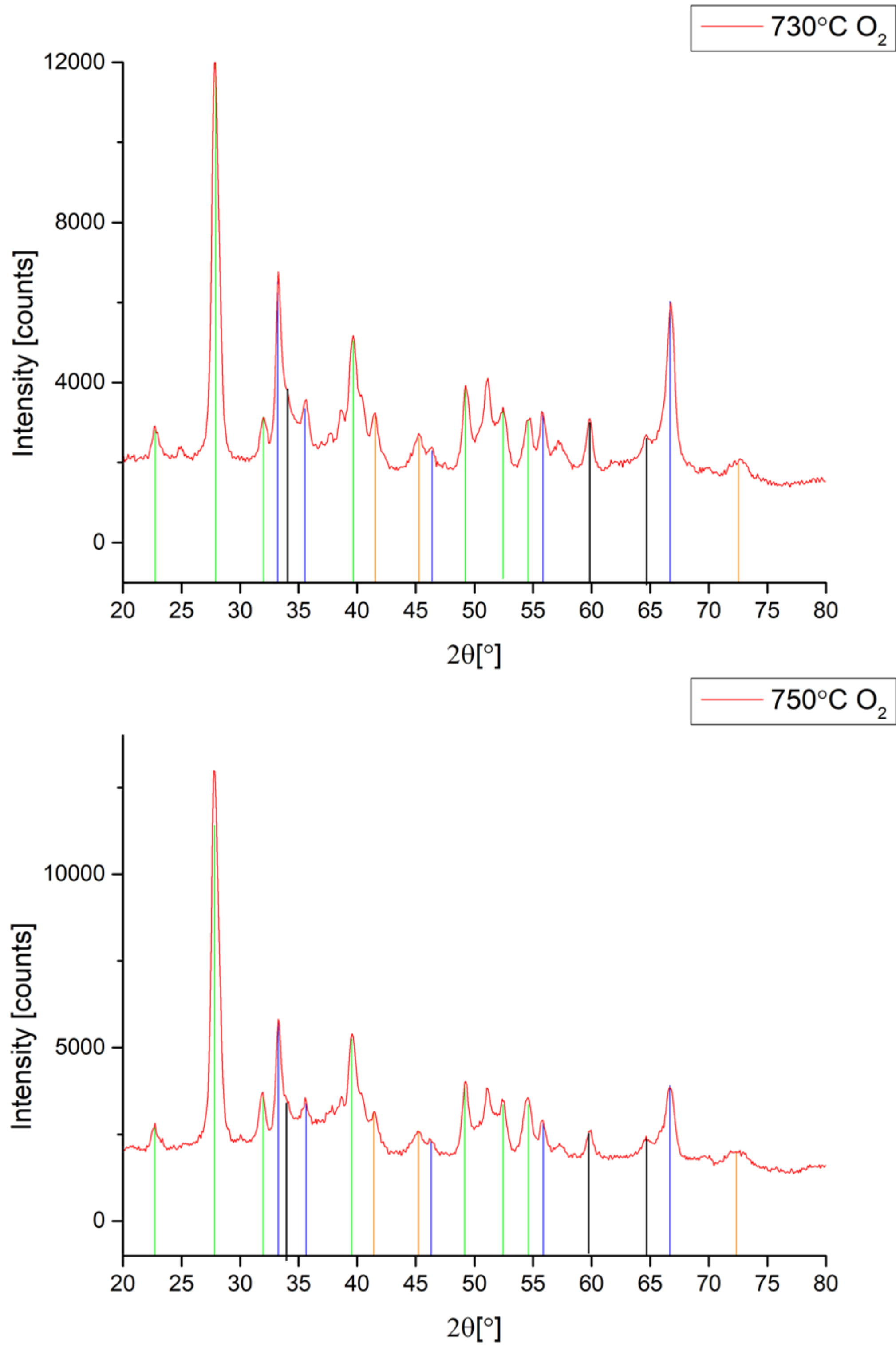

Figure 3.19: The XRD pattern of the oxidated YBCO thin film deposited at the substrate temperature 730°C and 750°C GREEN marked diffraction lines corresponds to $BaCO_3$. ORANGE marked diffraction lines corresponds to Cu_2O. BLUE marked diffraction lines corresponds to Y_2O_3. BLACK marked diffraction lines corresponds to $Y_2Ba_1Cu_1$.

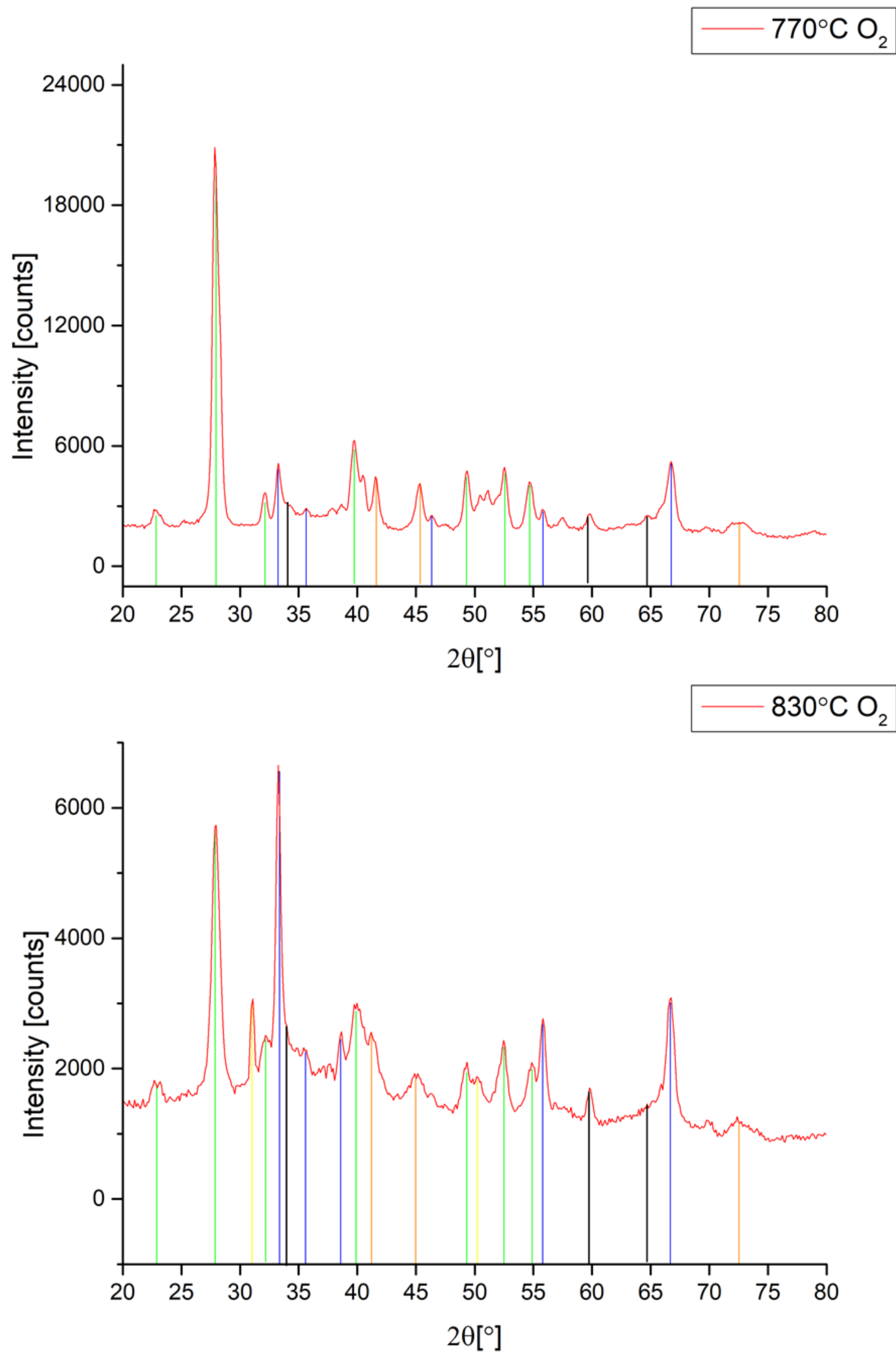

Figure 3.20: The XRD pattern of the oxidated YBCO thin film deposited at the substrate temperature 770°C and 830°C GREEN marked diffraction lines corresponds to $BaCO_3$. ORANGE marked diffraction lines corresponds to Cu_2O. BLUE marked diffraction lines corresponds to Y_2O_3. Yellow marked diffraction lines corresponds to BaO_2. BLACK marked diffraction lines corresponds to $Y_2Ba_1Cu_1$.

3.5 Characterization of Superconductive Properties

Superconducting properties were measured in two ways. By measuring the electrical resistance or by measuring the response of the sample to external magnetic field. Measurements by both methods were performed on all oxidized samples.

The measurements of electrical resistance were performed by the four-point method. In the case of YBCO-based superconductors, there is a significant drop in electrical resistance when the critical temperature is reached (see Fig.3.21). The contacts were attached to the samples with silver paste (see Fig.3.22). The samples were gradually cooled from the room temperature to 10 K, and during this time a continuous resistance measurement took place. Nevertheless, infinite electrical resistance was measured for all samples and no temperature dependence was observed.

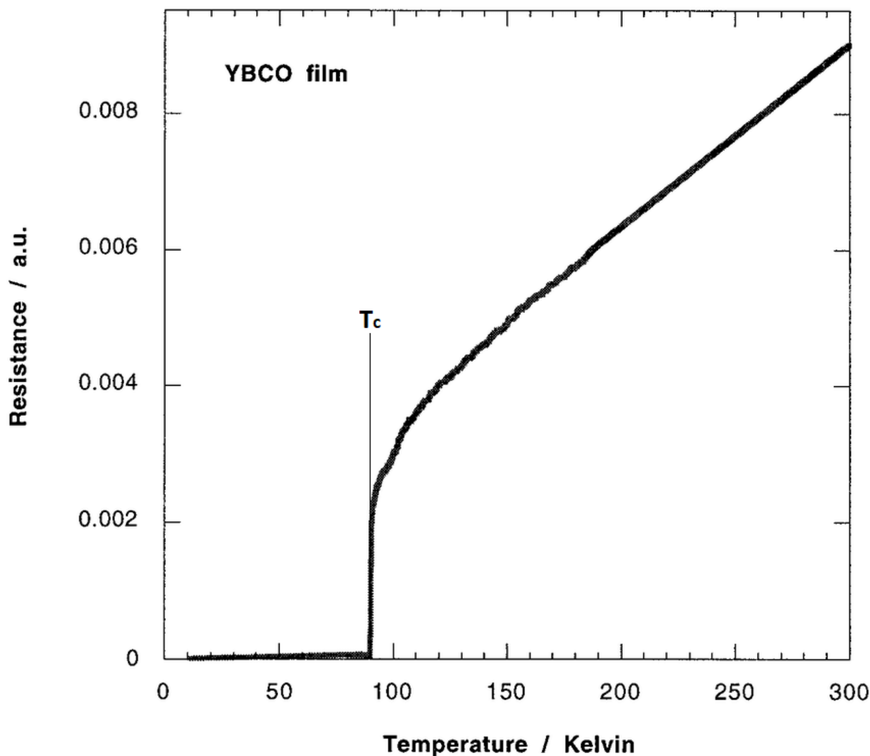

Figure 3.21: The typical temperature dependency of electrical resistance of superconductive YBCO film the critical temperature T_c is marked (after [51])

The reason for this result may be an imperfect connection of contacts or that there is no superconducting channel between the contacts. Imperfections in the connection of contacts can never be completely avoided. The layers also do not have to contain superconducting phases on their entire surface but only in separate parts.

To avoid these problems, measurements of the Meissner effect were performed. Meissner

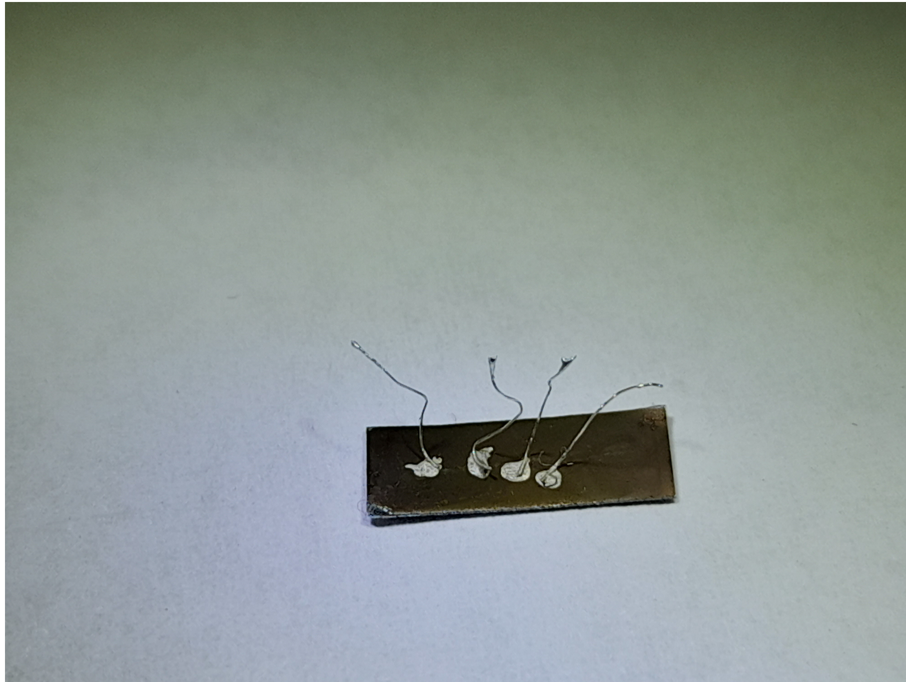

Figure 3.22: Attached contacts on a separate piece of sample prepared at the temperature of 770°C

effect consists in pushing the magnetic field out of the volume of superconductor, which results in levitation force acting between the magnetic field source and the superconductor (see Fig.3.23).

One large continuous volume is not required to observe the Meissner effect, and levitation itself is a non-contact phenomenon. Thanks to these properties, measurement of Meissner effect serves as a convenient method of measuring superconducting properties complementary to the four-point method used above. A control/reference sample manufactured by the German company Theva Dünnschichttechnik GmbH was used to ensure that at least a minimal levitation can be observed in the case of a thin superconducting film. The control tape had silver layer covering the surface as a mechanical protection of the underlaying superconducting layer. A neodymium magnet with a magnetic field of 0.3 T on the surface and a weight of 0.14 g was used for the measurement. The weight of the measured samples, including the control tape, is given in the table 3.8.

Table 3.8: Weight of the measured samples

Sample	Weight [g]
Control tape	0.22
730°C	0.10
750°C	0.11
770°C	0.09
830°C	0.11

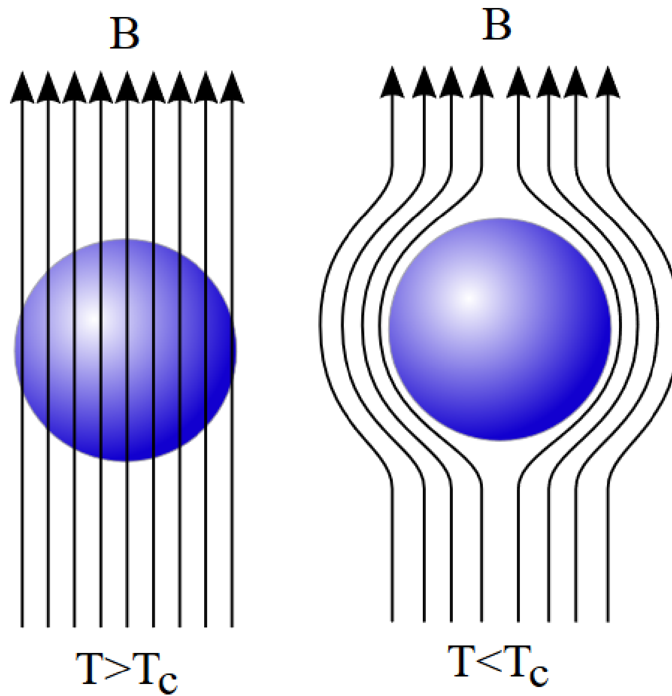

Figure 3.23: Schematic visualization of the Meissner effect. Situation observed for Type I superconductors [52]

The control measurement proved the possibility to observe the levitation of the magnet over the thin superconducting layer (see Fig.3.24) and it was therefore possible to verify by measuring the Meissner effect whether the prepared layer is at least partially superconducting or not. The Meissner effect of the thin film is so strong that it also allowed the control tape to hold itself levitating, as shown in Fig. 3.25. Unfortunately, no levitation was observed on all prepared samples (see Fig.3.26).

Negative results of the levitation and conductivity measurements implicate the conclusion that the prepared samples contain no or only very little of the desired superconductive $Y_1Ba_2Cu_3$ phase. This conclusion is conformal with the results of XRD analysis. At the conclusions of this thesis, the procedures are proposed how to modify the deposition process in order to achieve the superconducting thin films.

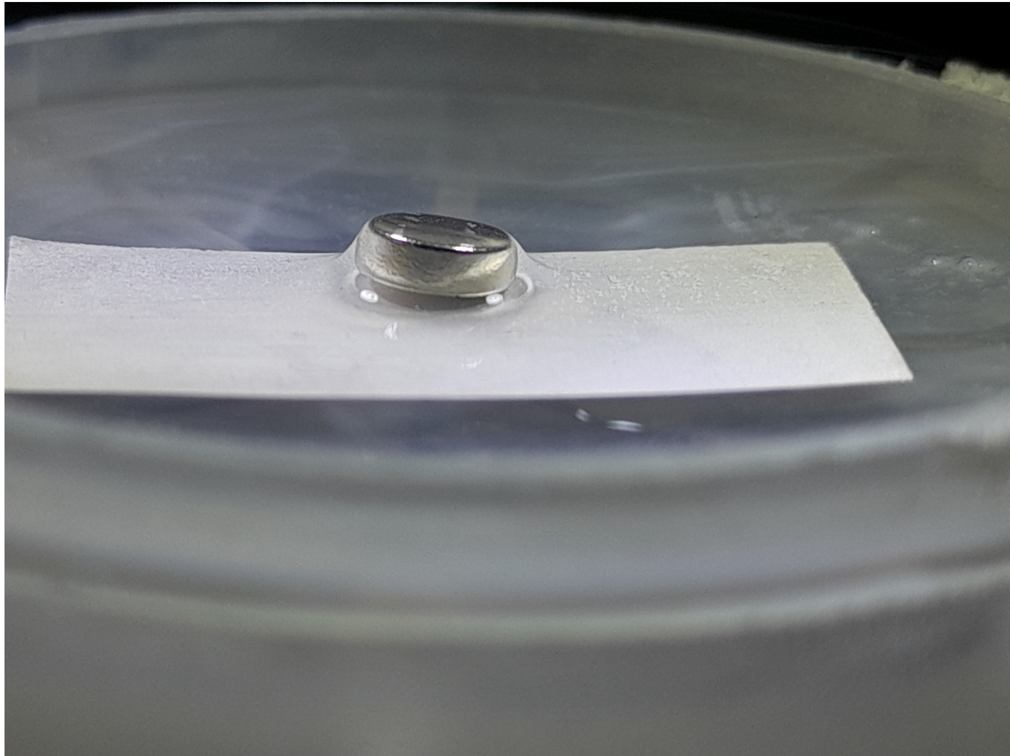

Figure 3.24: Picture of the magnet levitating over the control tape

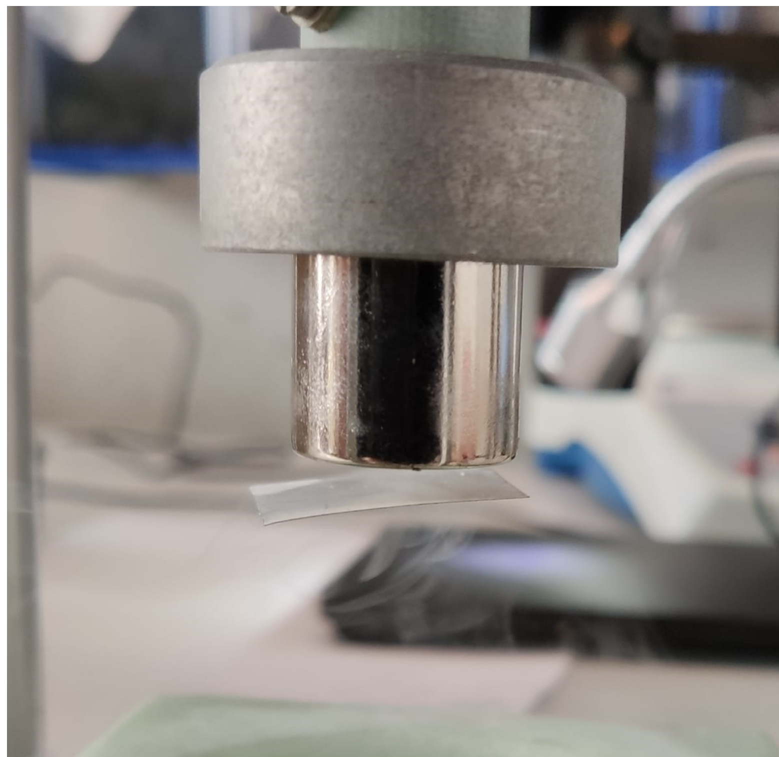

Figure 3.25: Picture of the control tape holding itself levitating below the permanent magnet

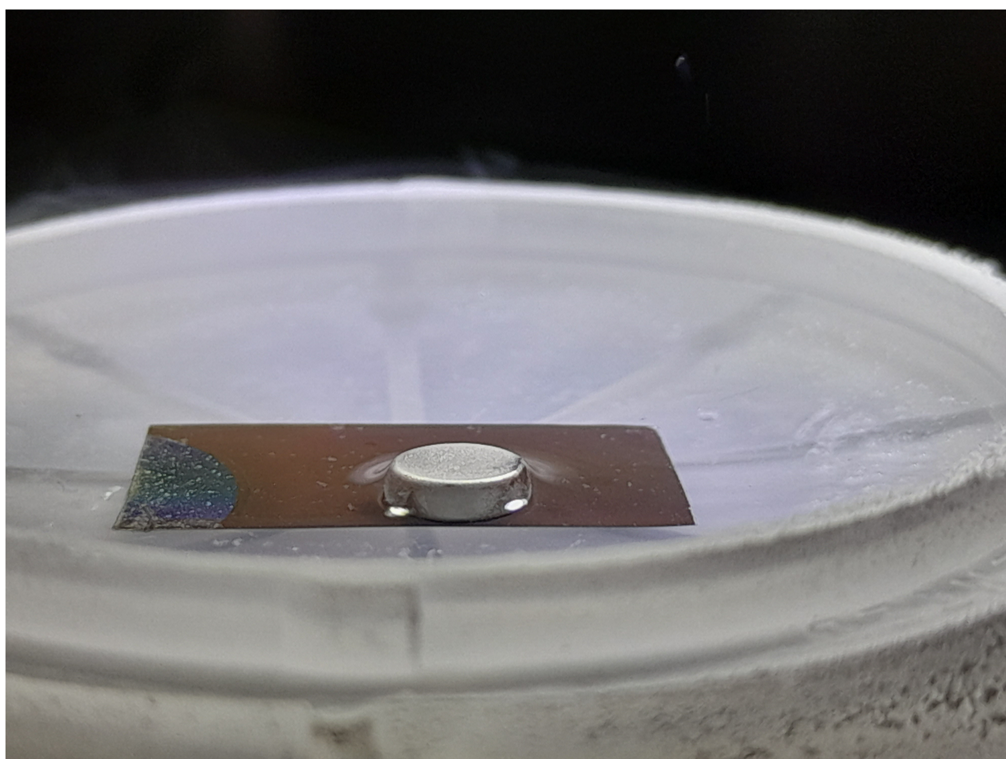

Figure 3.26: Picture of the magnet not levitating over the sample YBCO layer prepared at the temperature $770°C$

4 Conclusions

The first chapter provides introduction specifying the goals of this thesis. The second chapter is then devoted to detail theoretical basis needed to fully understand procedures used in the preparation and analysis of the studied HTS layers prepared by IJD method. First, the IJD itself is introduced and the physical phenomena involved are described, starting with the the interaction of electrons with the target which results in ablation of the target mass and converting it to plasma state. After creating the plasma from the target, a propagation of this plasma is described. The plasma arriving to the substrate condenses, and the thin film begins to form. Growth of the film layer and the ways in which its various properties can be examined in detail are described in the following section. The last section of the theoretical introduction deals with REBCO based high-temperature superconductors. Their crystalline structure is presented and the main issues associated with the preparation of these materials are discussed. The most important for the possibility of using this superconductors in practice is preparing them in a correct chemical composition, including oxygen content, and orient their crystalline structure correctly in accordance with their anisotropic superconducting properties.

The third, experimental chapter, constituting the main part of the thesis, describes then the conditions applied in preparation of several tested sets of samples and the achieved results. Each of these series of samples was designed and prepared with aim to analyse different property of the studied HTS films. Gradually, the deposition parameters were optimized on the basis of the obtained data, in order to achieve the best possible resulting layer.

The first set of deposition parameters optimized involved the acceleration voltage and the distance between the target and the substrate. The optimal distance between the target and the substrate was chosen to be around 110 mm, based on the experience with previous sample preparations and results of a detailed literature search. Three different samples were then prepared for the acceleration voltage examination. The value of the accelerating voltage of 14 kV appeared to be

the ideal value to be used in further investigations. The values of the accelerating voltage and the distance between the target and the substrate have since been fixed for all further iterations of the sample preparation procedure.

The next two sections are devoted to testing the influence of target properties on the structure and morphology of the prepared layers. The investigated parameters of targets involved their density and chemical composition. The density of the target affects the penetration depth of the electron in the ablation process. This effectively changes the amount of material deposited by a single pulse of electrons and thus the density of the plasma that is used to deposit the layer itself. This affects the growth rate of the film and also the film surface morphology due to a possible change in the formation of "droplets". For the analysis of these properties, a series of 9 target samples with different mass densities was prepared; the other deposition parameters were fixed. The density of the targets ranged from 3.8 g/cm^3 to 5.6 g/cm^3. The resulting layer thickness was measured by the confocal microscope and was found to range from 104 nm to 205 nm, the value corresponding well with the theory. The images from SEM were analyzed by ImageJ software and used to investigate film surface morphology. From the obtained data, there is no strong obvious dependence observed between the target density and the change in particle size or amount of the "droplets" presented on the surface. For further sample preparations, the highest possible target density was chosen. This decision was based on the literature results as well as on experience with mechanical handling of the targets during deposition, because in general, the targets with lower mass densities exhibited larger tendencies to crack during the deposition.

The chemical composition of the target is expected to affect the resulting composition of the prepared films, too. A series of targets with different chemical compositions close to the required composition Y123 was prepared, and a total amount of 7 samples with the same deposition parameters was prepared. Transport coefficients were calculated based on EDS analysis of the targets before deposition, targets after deposition, and the prepared layers. From the obtained data, it was found that during deposition the layer is enriched with yttrium and, conversely, the layer is depleted of barium.

The last prepared series of samples used the optimised parameters from the previous step, and focused on examining the crystalline structure of the prepared films. In HTS thin films, the phase growth is influenced mainly by the chemical composition of the arriving mass mixture, the substrate temperature and the substrate composition, crystalline structure and its orientation. A series of 4 samples on different substrates was prepared for the substrate influence analysis. For

further analyses, BruTape was chosen for its practical use in industry. To investigate the effect of the substrate temperature, a series of 6 samples was prepared at the temperatures ranging from 700°C to 830°C, and the set was completed by a control layer deposited at room temperature. The desired phase transition to ternary phases occurred in the samples deposited at substrate temperatures above 730°C. Unfortunately, the desired superconducting phase $Y_1Ba_2Cu_3$ was not found in any of the examined samples. Samples in which a phase transition was observed were then oxidized with aim to increase the oxygen content. This additional oxidation led to partial decomposition of less thermally stable phases into precursors of which the investigated material consists.

Superconducting properties of the oxidized samples were analyzed by means of electrical resistance measurements and by measuring the Meissner effect. These measurements again confirmed that the prepared HTS films samples are not showing superconducting properties, in agreement with the previous XRD analysis.

To prepare the desired REBCO superconducting layers using IJD, it will be necessary to precisely adjust the chemical composition of the films, which in the tested samples did not exactly match the required $Y_1Ba_2Cu_3$ stoichiometry. This adjustment can be made in two ways. The first possible one is to adjust the chemical composition of the targets so that the resulting film has the desired composition. The required chemical composition of the targets can be calculated from the values of the transport coefficients holding for the considered deposition conditions. At present, a second series of targets is prepared, fabricated according to these requirements, and preparation of the HTS layers is in progress. The second way how to achieve the required chemical composition of the layers is to increase the accelerating voltage, increasing thus the energy of the electron beam and ensuring stoichiometrically accurate material transfer between the target and the layer.

List of abbreviations

IJD Ionized Jet Deposition

HTS High temperature superconductor

YBCO Yttrium barium copper oxide that displays high temperature superconductivity

REBCO General group of rare-earth barium copper oxides that displays high temperature superconductivity

PVD Physical vapor deposition

SEM Scanning electron microscopy

EDS Energy dispersive spectroscopy

AFM Atomic force microscopy

XRD X-ray diffraction

XPS X-ray photoelectron spectroscopy

BCS theory Bardeen-Cooper-Schrieffer theory of superconductivity

Y123,Y143,Y152,Y211,Y358 Specific chemical phases in the system of yttrium barium copper oxide; the numbers indicates the stoichiometry of the system, for example Y123 stands for $Y_1Ba_2Cu_3O_{7-x}$

List of Figures

2.1 Schematic of channel-spark electron beam source; in the picture, K marks the hollow cathode, A - anode, C - capacitor, HV - the negative port of high voltage generator, T - target, S - substrate, and D - dielectric tube. [6] 8

2.2 Schematic view of IJD source [8]; the letters A,B,C and D indicate electrical connections (B, D) and groundings (A, C) 10

2.3 Schematics of hollow cathode effect; 1-hollow cathode, 2-grounded anode, 3- area of positive charge near the walls, 4-plasma channel, 5-electron trajectory, A,C-electric connections, D-diameter of the hollow cathode, d1,d2,d-characteristic distances [9] . 11

2.4 Paschen curve (calculated after Rel. 2.1) providing dependence of the breakdown voltage on the product of pressure and distance [10] 12

2.5 Picture of the double layer emitted from the hollow cathode; the negative charge region appears darker than the positive charge ones, due to the greater emission of light photons by positive ions comparing the photon emission from the negative electronic cloud [13] 13

2.6 Schematic of the plasma plume ablated by the IJD source from the target (green)[8] 14

2.7 Normalised absorbed power of electron beam along the depth below the target surface z [11] 16

2.8 Normalized angular distribution of target material ablated by IJD source [11] 17

2.9 The typical normalized distribution of the growing film thickness as function of the deviation from the IJD plasma plume axis (typically parallel to the sample surface normal) [11] 17

2.10 The four phases of plasma plume propagation described in text [16] 19

2.11 Graph of directional velocity v and thermal velocity v_T in dependence on normalized distance; the value L_0 is given by the intersection of both velocity curves [16] 20

2.12 Scheme of the surface tension components acting at the growing film interface [19] . 22

2.13 Schematic picture of the growth modes of thin films: Frank-van der Merwe mode (a), Volmer-Weber mode (b) and Stranski-Krastanov mode (c) [18] 23

2.14 SEM image of YBCO thin film prepared by IJD method; "droplets" are clearly visible 25

2.15 SEM micrograph of the fracture of Al_2O_3 thin film deposited on monocrystalline silicon wafer; the regions belonging respectively to the film and the substrate are indicated 26

2.16 Schematic of SEM; in addition to the secondary electrons detector, an X-ray detector can be used too, providing EDS analysis [20] 26

2.17 Scheme of interaction of primary electron beam with a solid sample [20] 27

2.18 Schematic of AFM measurement with optical detection of the cantilever bend [23] . 28

2.19 Schematic of measurement of thin film by grazing incidence angle XRD [27] 30

2.20 Schematic of XPS setup [29] 30

2.21 Schematic illustration of the confocal microscopy setup. [31] 31

2.22 Elementary cell of YBCO crystalline structure, the oxygen, barium, copper and yttrium atoms are marked in red, purple, blue and green color, respectively [35] . . . 33

2.23 Influence of oxygen stoichimetry on the critical temperature of YBCO superconductors [36] 34

2.24 The ternary phase diagram of BaO-CuO-Y_2O_3 system [42] 35

3.1 SEM images of the films prepared using acceleration voltage 10 kV (top left), 12 kV (top right) and 14kV (bottom); Tescan MAIA3 scanning electron microscope 39

3.2 Mass densities of the prepared targets and the main preparation parameters (furnace temperature and the dwell time) 40

3.3 Example of 2D (left) and 3D (right) picture of prepared layer surface recorded by confocal microscope; target with mass density 5.4g/cm^3 used for deposition; edge of the layer is clearly visible 42

3.4 Example of thickness profile of the film grown with target of the mass density 5.4 g/cm^3 42

3.5 Normalized penetration depth depending on the density of the target (full line) combined with the experimentally obtained thickness of the grown films (full squares with ESD indicated) 43

3.6 Example of the image processing steps applied in the surface topology analysis of the prepared layers performed by ImageJ software; the used target density 4.84 g/cm^3. Original SEM micrograph (top left), selected area for examination (top right), B/W converted picture with contrast threshold set (bottom left), isolated particle boundaries (bottom right) 45

3.7 Original SEM snaps of layers prepared from targets of different density. 46

3.8 Example of the obtained distribution of the marked elements in the prepared thin film and in the substrate. The film was prepared from the $Y_1Ba_2Cu_3O_x$ target; the SEM view of the surface is shown on the left-most picture 48

3.9 Picture of the thin film with the arrow pointing to the edge where the EDS was measured 48

3.10 Example of the data obtained from the EDS analysis for the sample prepared from the $Y_1Ba_2Cu_3O_x$ target 49

3.11 The atomic percentage of Y,Ba and Cu obtained from the EDS data for each initial stoichiometric composition and indicated type of measurement (on the fresh target, on the prepared layer, and on the target after IJD deposition). 51

3.12 The XRD pattern of monocrystalline YBCO bulk, used as the standard, measured in Bragg-Brentano geometry; the bulk surface normal parallel to the scattering vector. 53

3.13 Substrates in the sample holder before deposition (left), and after deposition (right) 54

3.14 The XRD pattern of YBCO thin film on Si (111) and LaAlO$_3$ (100) wafer. GREEN marked diffraction lines corresponds to $BaCO_3$. ORANGE marked diffraction lines corresponds to Cu_2O. BLUE marked diffraction lines corresponds to Y_2O_3. 56

3.15 The XRD pattern of YBCO thin film on BruTape and on OxTape. GREEN marked diffraction lines corresponds to $BaCO_3$. ORANGE marked diffraction lines corresponds to Cu_2O. BLUE marked diffraction lines corresponds to Y_2O_3. BLACK marked diffraction lines corresponds to $Y_2Ba_1Cu_1$. Unmarked diffraction lines belong to the substrate 57

3.16 The XRD pattern of YBCO thin film deposited at the substrate temperature RT and 700°C GREEN marked diffraction lines corresponds to $BaCO_3$. ORANGE marked diffraction lines corresponds to Cu_2O. BLUE marked diffraction lines corresponds to Y_2O_3. BLACK marked diffraction lines corresponds to $Y_2Ba_1Cu_1$. RED marked diffraction lines corresponds to $CuYO_2$ 60

3.17 The XRD pattern of YBCO thin film deposited at the substrate temperature 730°C and 750°C GREEN marked diffraction lines corresponds to $BaCO_3$. ORANGE marked diffraction lines corresponds to Cu_2O. BLUE marked diffraction lines corresponds to Y_2O_3. BLACK marked diffraction lines corresponds to $Y_2Ba_1Cu_1$. RED marked diffraction lines corresponds to $CuYO_2$ . . . 61

3.18 The XRD pattern of YBCO thin film deposited at the substrate temperature 770°C and 830°C GREEN marked diffraction lines corresponds to $BaCO_3$. ORANGE marked diffraction lines corresponds to Cu_2O. BLUE marked diffraction lines corresponds to Y_2O_3. BLACK marked diffraction lines corresponds to $Y_2Ba_1Cu_1$. RED marked diffraction lines corresponds to $CuYO_2$ . . . 62

3.19 The XRD pattern of the oxidated YBCO thin film deposited at the substrate temperature 730°C and 750°C GREEN marked diffraction lines corresponds to $BaCO_3$. ORANGE marked diffraction lines corresponds to Cu_2O. BLUE marked diffraction lines corresponds to Y_2O_3. BLACK marked diffraction lines corresponds to $Y_2Ba_1Cu_1$. 64

3.20 The XRD pattern of the oxidated YBCO thin film deposited at the substrate temperature 770°C and 830°C GREEN marked diffraction lines corresponds to $BaCO_3$. ORANGE marked diffraction lines corresponds to Cu_2O. BLUE marked diffraction lines corresponds to Y_2O_3. Yellow marked diffraction lines corresponds to BaO_2. BLACK marked diffraction lines corresponds to $Y_2Ba_1Cu_1$. . . . 65

3.21 The typical temperature dependency of electrical resistance of superconductive YBCO film the critical temperature T_c is marked (after [51]) . . . 66

3.22 Attached contacts on a separate piece of sample prepared at the temperature of 770°C 67

3.23 Schematic visualization of the Meissner effect. Situation observed for Type I superconductors [52] . . . 68

3.24 Picture of the magnet levitating over the control tape . . . 69

3.25 Picture of the control tape holding itself levitating below the permanent magnet . . 69

3.26 Picture of the magnet not levitating over the sample YBCO layer prepared at the temperature 770°C . . . 70

List of Tables

2.1 Characteristic IJD pulse parameters (unpublished data Noivion srl. and [11]) 13

3.1 Deposition parameters for the set of samples used in examination of acceleration voltage influence 38

3.2 The film thickness grown from the targets with indicated mass densities; identical IJD growth conditions were applied for all the prepared films 42

3.3 The characteristics of surface droplets obtained from topological analysis of SEM micro-graphs shown in Figure 3.7 46

3.4 Transport coefficients for Y, Ba and Cu related to the targets´ composition before deposition 49

3.5 Transport coefficients for Y, Ba and Cu related to the targets´ composition after deposition. 50

3.6 Deposition parameters for the set of samples used in examination of the substrate influence 54

3.7 Deposition parameters for the set of samples used for examination of the substrate temperature influence 58

3.8 Weight of the measured samples 67

References

[1] J. Skocdopole et. al. Transport coefficients in Y-Ba-Cu-O system for ionized jet deposition method. *IEEE Transactions on Applied Superconductivity*, 31(5):1–3, 2021.

[2] M. Lojka et. al. Effect of target density on the surface morphology of Y-Ba-Cu-O thin films prepared by ionized jet deposition. *IEEE Transactions on Applied Superconductivity*, 31(5):1–5, 2021.

[3] T. Kostal. *Preparation and X-ray diffraction analysis of superconducting thin films deposited by IJD method.* CTU in Prague, bachelor thesis, 2021.

[4] J. Skočdopole et. al. Influence of substrate temperature on the morphology and phase composition of thin films prepared from y-123 targets by the ijd method. *IEEE Trans. Appl. Supercond.*, 33(5):1–4, 2023.

[5] F.N. Werfel et. al. Experiments of superconducting maglev ground transportation. *IEEE Trans. Appl. Supercond*, 26(3):1–5, 2016.

[6] M. Nistor et. al. (zrsn)tio$_4$ thin films for application in electronics. *Applied Surface Science*, 247:169–174, 2005.

[7] T. Witke et. al. Channel spark discharges for thin film technology. *IEEE Transactions on Plasma Science*, 25(4):758–762, 1997.

[8] J. Skocdopole. *IJD deposition of ultra-hard thin layers onto substrates of high-alloy steels - an application in medicine study.* CTU in Prague, master thesis, 2017.

[9] A. Metel V. Kolobov. Glow discharges with electrostatic confinement of fast electrons. *Journal of Physics D Applied Physics*, 48(23):1–19, 2015.

[10] G. Giacomo. Paschen's law in extreme pressure and temperature conditions. *IEEE Transactions on Plasma Science*, 47(3):1641–1647, 2019.

[11] G. Müller et. al. Thin film deposition by means of pulsed electron beam ablation. In *Science and Technology of Thin Films*, pages 89–119. World scientific, 1995.

[12] M.A. Raadu and J.J. Rasmussen. Dynamical aspects of electrostatic double layers. *Astrophys Space Sci*, 144:43–71, 1988.

[13] I.G. Mikellides et. al. Model of the plasma potential distribution in the plume of a hollow cathode. In *40th AIAA/ASME/SAE/ASEE Joint Propulsion Conference and Exhibit*, 2004.

[14] D.E. Gray B.H. Billings. *American Institute of Physics Handbook*. New York : McGraw-Hill, third edition, 1972.

[15] S. Schiller et.al. *Elektronenstrahltechnolog*. Forschungsinstitut Manfred von Ardenne, Dresden VEB Verlag, 1976.

[16] S.H. Kolagani M.D. Strikovski, J. Kim. Plasma energetics in pulsed laser and pulsed electron deposition. In *Springer Handbook of Crystal Growth*, pages 1193–1211. Springer Berlin Heidelberg, 2010.

[17] J. Miller M.D. Strikovski. Pulsed laser deposition of oxides: Why the optimum rate is about 1 Å per pulse. *Appl. Phys. Lett.*, 73(12):1733–1735, 1998.

[18] A.S. Parshin L. Kalvoda. *Vybraná témata z fyziky povrchů*. Nakladatelství ČVUT Praha, 2000.

[19] N. Kaiser. Review of the fundamentals of thin-film growth. *Appl. Opt.*, 41(16):3053–3060, 2002.

[20] N. Marturi. *Vision and visual servoing for nanomanipulation and nanocharacterization in scanning electron microscope*. Universite de Franche-Com, 2013.

[21] S. Ebnesajjad. Surface and material characterization techniques. In *Surface Treatment of Materials for Adhesive Bonding*, pages 39–75. William Andrew Publishing, 2014.

[22] G. Binnig F. Ohnesorge. True atomic resolution by atomic force microscopy through repulsive and attractive forces. *Science*, 260(5113):1451–1456, 1993.

[23] O. Marti. Afm instrumentation and tips. In *Handbook of Micro/Nanotribology*, pages 81–144. CRC, Boca Raton, 1999.

[24] J. Skocdopole. *Preparation of thin layers by IJD method and characterization of their physical-chemical properties.* CTU in Prague, bachelor thesis, 2015.

[25] I. Kraus. *Úvod do strukturní rentgenografie.* Academia, 1985.

[26] S. Dietrich and A. Haase. Scattering of x-rays and neutrons at interfaces. *Physics Reports*, 260(1):1–138, 1995.

[27] L. C. Tracy et. al. Measurement of uo_2 surface oxidation using grazing-incidence x-ray diffraction: Implications for nuclear forensics. *Journal of Nuclear Materials*, 502:68–75, 2018.

[28] J. Skocdopole. *Construction of system for deposition of thin films by IJD method and trial deposition of chosen materials.* CTU in Prague, research thesis, 2016.

[29] D. Regonini. *Anodised TiO2 Nanotubes: Synthesis, Growth Mechanism and Thermal Stability.* University of Bath, PhD. thesis, 2008.

[30] J. B. Pawley. *Handbook Of Biological Confocal Microscopy.* Springer, Boston, MA, 2006.

[31] S. Mahmudi-Azer et. al. Tracing intracellular mediator storage and mobilization in eosinophils. *Methods in molecular medicine*, 56:367–381, 2001.

[32] J. R. Schrieffer. *Handbook of High-Temperature Superconductivity.* Springer-Verlag New York, 2007.

[33] Anant V. Narlikar. *High Temperature Superconductivity 1.* Springer Berlin, Heidelberg, 2004.

[34] F. Majewski. Superconducting materials. In *Encyclopedia of Materials: Technical Ceramics and Glasses*, pages 151–161. Elsevier, 2021.

[35] Structure type 071: Yba2cu3o7 (ybco). `http://som.web.cmu.edu/structures/S071-YBCO.html`. Accessed: 12-06-2021.

[36] A. Mourachkine. *High-Temperature Superconductivity in Cuprates.* Springer, Dordrecht, 2002.

[37] S. Katano et. al. Crystal structure of the tetragonal superconductor $CaLaBaCu_3O_x$ ($6.69 \leq x \leq 6.94$). *Physica C: Superconductivity*, 217(1):73–78, 1993.

[38] H. S. Cornejo et. al. Texture and magnetic anisotropy of $YBa_2Cu_3O_{7-x}$ film on MgO substrate. *Journal of Materials Science: Materials in Electronics*, 31(1):21108–21117, 2020.

[39] P. Zhao et. al. Fabrication of ybco film patterns and their properties. *Superconductor Science and Technology*, 21(12):1–4, 2008.

[40] M. Ohmukai et. al. Post-deposition cooling in oxygen is critical for $YBa_2Cu_3O_7$ films deposited by eclipse pulsed laser deposition method. *Braz. J. Phys.*, 31(1):30–33, 2001.

[41] A. Earnshaw N.N. Greenwood. Scandium, yttrium, lanthanum and actinium. In *Chemistry of the Elements*, pages 944–953. Butterworth-Heinemann, 1997.

[42] D.M. De Leeuw et. al. Compounds and phase compatibilities in the system y_2o_3-bao-cuo at 950°c. *Physica C: Superconductivity*, 152(1):39–49, 1988.

[43] O. Ozturk et. al. Investigation of structural, superconducting and mechanical properties of co/cu substituted ybco-358 ceramic composites. *Journal of Materials Science: Materials in Electronics*, 30(8):7400–7409, 2019.

[44] P. Zhao et. al. Ternary phase relation on preparation of $YBa_2Cu_3O_{7-\delta}$ films by laser cvd. *Key Engineering Materials*, 484(1):183–187, 2011.

[45] A. Gambardella et. al. A comparative study of the growth dynamics of zirconia thin films deposited by ionized jet deposition onto different substrates. *Surface and Coatings Technology*, 337(1):306–312, 2018.

[46] S. Nekvinda. *Preparation and analysis of High Entropy Alloys thin films deposited by Ionized Jet Deposition method.* CTU in Prague, bachelor thesis, 2019.

[47] A. Knizhnik et. al. Interrelation of preparation conditions, morphology, chemical reactivity and homogeneity of ceramic ybco. *Physica C: Superconductivity*, 400(1):25–35, 2003.

[48] H.U. Habermeier et. al. Y-ba-cu-o high temperature superconductor thin film preparation by pulsed laser deposition and rf sputtering: A comparative study. *Physica C: Superconductivity*, 180(1):17–25, 1991.

[49] M.Lojka, Private Communication, 2022.

[50] V I Dediu et. al. Deposition of $MBa_2Cu_3O_{7-x}$thin films by channel-spark method. *Superconductor Science and Technology*, 8(3):160–164, 1995.

[51] M. Abrecht et. al. Surface optimization of $RBa_2Cu_3O_{7-\delta}$ (R = Y, Nd) epitaxial high T_c films for in situ photoemission studies. *Surface Review and Letters*, 4(1):495–500, 2000.

[52] Meissner Effect and Lorentz Force Paradox. `https://physics.stackexchange.com/q/566117`. Accessed: 17-07-2020.